A Novel Facet of Carbonyliron-Diene Photochemistry: The η^4-*s-trans* Isomer of the Classical $Fe(CO)_3(\eta^4$-*s-cis*-1,3-butadiene) Discovered by Time-Resolved IR Spectroscopy and Theoretically Examined by Density Functional Methods

Vinzenz Bachler,* Friedrich-Wilhelm Grevels,* Klaus Kerpen, Gottfried Olbrich, and Kurt Schaffner

Max-Planck-Institut für Strahlenchemie, Stiftstrasse 34-36, Postfach 10 13 65, D-45413 Mülheim an der Ruhr, Germany

Received September 18, 2002

The photolysis of $Fe(CO)_3(\eta^4$-*s-cis*-1,3-butadiene) (**1**) and $Fe(CO)_4(\eta^2$-1,3-butadiene) (**2**), formerly studied in low-temperature matrixes, is reexamined in cyclohexane solution at ambient temperature using time-resolved IR spectroscopy in the ν(CO) region. Flash photolysis of **2** ($\lambda_{exc} = 308$ nm) generates $Fe(CO)_3(\eta^4$-*s-trans*-1,3-butadiene) (**5**) as a transient product, which then rearranges to form the classical η^4-*s-cis*-1,3-butadiene complex **1**. Species **5**, previously addressed as the coordinately unsaturated $Fe(CO)_3(\eta^2$-1,3-butadiene) (**3**), is also photogenerated from **1**, in this case along with the very short-lived CO loss fragment $Fe(CO)_2(\eta^4$-1,3-butadiene) ($\tau < 4$ μs under CO atmosphere). It decays by temperature-dependent first-order kinetics ($\tau = 13$ ms at 25 °C; $\Delta H^{\ddagger} = 17.3$ kcal·mol^{-1}) with nearly complete recovery of **1**. According to density functional calculations at the BP86 level of theory, **5** resides in a distinct energy minimum, 20.3 kcal·mol^{-1} above **1** and separated from it by a barrier of 15.0 kcal·mol^{-1}. Its computed structure involves a diene dihedral angle of 129°. Species **3** (with a diene dihedral angle of −150.1°), by contrast, is predicted to exist in a rather flat minimum, which makes it too short-lived for detection with our instrumentation. Flash photolysis of $Fe(CO)_5$ generates the very short-lived (<1 μs) doubly unsaturated $Fe(CO)_3$(solv) species in addition to the familiar $Fe(CO)_4$(solv) fragment ($\tau = 10-15$ μs), $Fe_2(CO)_9$ being the ultimate product in the absence of potential trapping agents other than CO. Deliberate contamination of the system with water gives rise to the formation of $Fe(CO)_4(H_2O)$ as a longer lived transient (ca. 1 ms). In the presence of 1,3-butadiene, both **2** and **5** appear almost instantaneously. The latter decays, again in the millisecond time range, with formation of **1**, thus providing clear evidence of a single-photon route from $Fe(CO)_5$ to **1** in addition to the established two-photon sequence via the monosubstituted complex **2**.

Introduction

Tricarbonyl(η^4-diene)iron complexes are accessible by various routes[1] and have found a wide range of applications in metal-assisted organic syntheses.[2] The parent member of this class of compounds, $Fe(CO)_3(\eta^4$-1,3-bd) (**1**, bd = butadiene), was first prepared by heating $Fe(CO)_5$ and 1,3-butadiene in a pressure vessel.[3,4] An alternative photochemical procedure, explored and elaborated in this laboratory, takes advantage of the high efficiency of photolytic CO substitution under thermally mild conditions and affords high yields of **1** in hydrocarbon solution at ambient temperature.[5] The overall process was formulated as a sequence of two consecutive photochemical steps, Scheme 1, involving the intermediate formation of the monosubstituted $Fe(CO)_4(\eta^2$-1,3-bd) (**2**), which is independently accessible from $Fe_2(CO)_9$ and 1,3-butadiene.[6]

The thermal stability of **1** and the existence of the analogous 1,3-cyclohexadiene complex led to the proposal that the 1,3-diene ligand is η^4-coordinated in its *s-cis* conformation.[7] This has been verified by a single-crystal X-ray structure analysis of **1**,[8] which, moreover, revealed a square-pyramidal coordination geometry with the C=C units of the diene in two basal positions. These characteristics were found as recurrent features in the structures of many other $Fe(CO)_3(\eta^4$-1,3-diene) compounds and in the related $Fe(CO)(\eta^4$-1,3-diene$)_2$ complexes as well.[9,10]

* To whom correspondence should be addressed. E-mail: grevels@mpi-muelheim.mpg.de.

(1) Knölker, H.-J. *Chem. Rev.* **2000**, *100*, 2941−2961.
(2) Grée, R.; Lellouche, J. P. *Adv. Metal-Org. Chem.* **1995**, *4*, 129−273.
(3) Reihlen, H.; Gruhl, A.; v. Hessling, G.; Pfrengle, O. *Liebigs Ann. Chem.* **1930**, *482*, 161−182.
(4) King, R. B. *Organometallic Syntheses, Vol. 1, Transition-Metal Compounds*; Academic: New York, 1965; pp 128−129.
(5) Koerner von Gustorf, E.; Pfajfer, Z.; Grevels, F.-W. *Z. Naturforsch. B* **1971**, *26*, 66−67.
(6) Murdoch, H. D.; Weiss, E. *Helv. Chim. Acta* **1962**, *45*, 1156−1161.
(7) Hallam, B. F.; Pauson, P. L. *J. Chem. Soc.* **1958**, 642−645.
(8) Mills, O. S.; Robinson, G. *Acta Crystallogr.* **1963**, *16*, 758−761.

10.1021/om020785c CCC: $25.00
Publication on Web 03/15/2003

Scheme 1

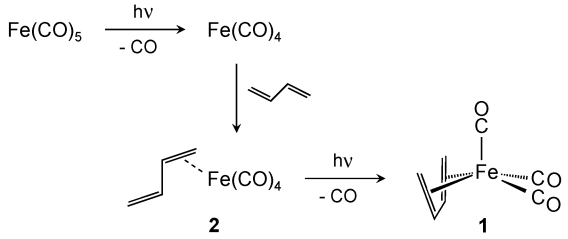

High yields of the latter compounds are accessible from photogenerated Fe(CO)$_3$(η^4-1,3-diene) by further CO photosubstitution occurring upon extended irradiation in the presence of excess diene.[5,11] Other photoinduced reactions of Fe(CO)$_3$(η^4-1,3-diene) complexes include CO/^{13}CO exchange,[12] metal-assisted diene−olefin coupling,[13,14] and CO substitution by phosphine ligands yielding Fe(CO)$_2$(η^4-1,3-diene)(L) derivatives,[12,15] whereas replacement of the diene plays only a minor role.[15]

Mechanistic aspects have been addressed in low-temperature matrix studies using conventional IR spectroscopy in the CO stretching vibrational region.[16,17] Photolysis of Fe(CO)$_4$(η^2-1,3-bd) (**2**) initially yields a tricarbonyliron intermediate, at that time assigned as the coordinately unsaturated species Fe(CO)$_3$(η^2-1,3-bd) (**3**), which upon continued irradiation is converted into Fe(CO)$_3$(η^4-1,3-bd) (**1**).[16] The same tricarbonyliron species is also generated by photolysis of **1**,[16,17] in this case along with the dicarbonyl fragment Fe(CO)$_2$(η^4-1,3-bd) (**4**), thus indicating that two primary photoprocesses of Fe(CO)$_3$(η^4-1,3-diene) complexes may be operative, detachment of CO and dechelation of the η^4-diene ligand.

The laser flash photolysis experiments, reported in the present paper, aim at elucidating the kinetics and reactivity of the above photoproducts of **1** and **2** in hydrocarbon solution at ambient temperature by means of time-resolved IR spectroscopy in the micro- and millisecond time domain. As a most interesting outcome, our experimental findings demand a reassignment of the tricarbonyliron species "Fe(CO)$_3$(η^2-1,3-bd)" (**3**) as a novel isomer of **1**, Fe(CO)$_3$(η^4-*s*-*trans*-1,3-bd) (**5**), which finds support from the results of a density functional theory (DFT) study. In this context we also examine the photofragmentation of Fe(CO)$_5$ in hydrocarbon solution in the presence and in the absence of 1,3-butadiene. As a noteworthy result of this part of the study, the doubly unsaturated species Fe(CO)$_3$(solv) is recognized as a single-photon product of Fe(CO)$_5$ in addition to the expected Fe(CO)$_4$(solv).[18]

Results and Discussion

Flash Photolysis of Fe(CO)$_3$(η^4-1,3-butadiene) (1). The electronic absorption spectrum of **1** exhibits a maximum at 282 nm (ϵ = 2550 L·mol^{-1}·cm^{-1}) as the only distinct feature on a steep declivity from the UV to longer wavelengths. It ends in a long tail absorption which extends into the visible region and is responsible for the yellow color of the complex. Concrete information on the underlying transitions is lacking, apart from the observation that the efficiency of both CO and diene photosubstitution decreases significantly on going from shorter to longer wavelengths. At 313 nm, for example, Φ_{CO} = 0.16 and Φ_{diene} = 0.015 were measured with trimethyl phosphite as the entering ligand.[15] Thus, flash photolysis of **1** at λ = 308 nm, using the XeCl excimer laser routinely available in our experimental setup, seems appropriate for the present time-resolved IR spectroscopic study. Most clear results were obtained under CO atmosphere, where the system proved largely reversible.[19]

Transient IR difference spectra in the ν(CO) region have been recorded in two time ranges, 100 μs (Figure 1) and 40 ms (Figure 2). The spectrum displayed in Figure 1A represents the situation at a time (1.5 μs) at which our instrumentation shows full response. In addition to the depletion pattern of the starting material **1** (2056, 1988, and 1980 cm^{-1}; cf. Table 1 for reference data), five product absorptions have emerged, which are readily grouped into two sets on the basis of their distinctly different decay kinetics, 2024/1962/1944 and 2002/1938 cm^{-1}.

The latter pair of bands is in close agreement with the data previously reported for the CO loss product of **1** in low-temperature matrixes (2009 and 1943 cm^{-1} in Ar; 1999 and 1936 cm^{-1} in Xe),[16] such that the assignment as the dicarbonyl fragment Fe(CO)$_2$(η^4-1,3-bd)(solv) (**4**) is straightforward. It decays very rapidly within a few microseconds with concomitantly occurring partial recovery of the depletion bands associated with **1**, as exemplarily illustrated in Figure 1B by the signals recorded at 2002 and 2056 cm^{-1}. Obviously, fragment **4** immediately takes up carbon monoxide from the CO-saturated solution to re-form a corresponding amount of the parent **1**, Scheme 2.[18,20]

The difference spectrum left behind after 4 μs (Figure 1C) comprises the aforementioned three-band pattern (marked as shaded areas) along with a weaker, new absorption which has emerged at 1920 cm^{-1} during the fast decay of **4**. It vanishes within a period of 25−30 μs, during which further recovery of depleted **1** takes place, as documented by the ΔA signals recorded at 1920 and 2056 cm^{-1}, respectively (Figure 1B). Apparently, a certain amount of **4** is temporarily trapped by a weakly binding agent present as an impurity in the solution, water being a likely candidate by analogy with similar observations made in our early investigations into the

(9) Krüger, C.; Tsay, Y.-H. *Angew. Chem.* **1971**, *83*, 250−251; *Angew. Chem., Int. Ed. Engl.* **1971**, *10*, 261.
(10) Whiting, D. A. *Cryst. Struct. Commun.* **1972**, *1*, 379−381.
(11) Koerner von Gustorf, E.; Buchkremer, J.; Pfajfer, Z.; Grevels, F.-W. *Angew. Chem.* **1971**, *83*, 249−250; *Angew. Chem., Int. Ed. Engl.* **1971**, *10*, 260−261.
(12) Warren, J. D.; Clark, R. J. *Inorg. Chem.* **1970**, *9*, 373−379.
(13) Kerber, R. C.; Koerner von Gustorf, E. A. *J. Organomet. Chem.* **1976**, *110*, 345−357.
(14) Grevels, F.-W.; Feldhoff, U.; Leitich, J.; Krüger, C. *J. Organomet. Chem.* **1976**, *118*, 79−92.
(15) Jaenicke, O.; Kerber, R. C.; Kirsch, P.; Koerner von Gustorf, E. A.; Rumin, R. *J. Organomet. Chem.* **1980**, *187*, 361−373.
(16) Ellerhorst, G.; Gerhartz, W.; Grevels, F.-W. *Inorg. Chem.* **1980**, *19*, 67−71.
(17) Astley, S. T.; Churton, M. P. V.; Hitam, R. B.; Rest, A. J. *J. Chem. Soc., Dalton Trans.* **1990**, 3243−3253.

(18) In the schemes, the solvent molecule(s) occupying the vacant coordination site(s) of the fragments Fe(CO)$_4$, Fe(CO)$_3$, Fe(CO)$_3$(η^2-1,3-bd) (**3**), and Fe(CO)$_2$(η^4-1,3-bd) (**4**) are omitted for the sake of conciseness. As regards the doubly unsaturated Fe(CO)$_3$, this species is formulated as Fe(CO)$_3$(solv) in the running text, since concrete information on the number of coordinated solvent molecules is lacking.
(19) Under argon or argon-diluted atmosphere (Ar/CO 9:1), the reversibility is diminished due to the formation of ill-defined, long-lived (>1 s) side products.
(20) The dotted arrows refer to processes of minor importance.

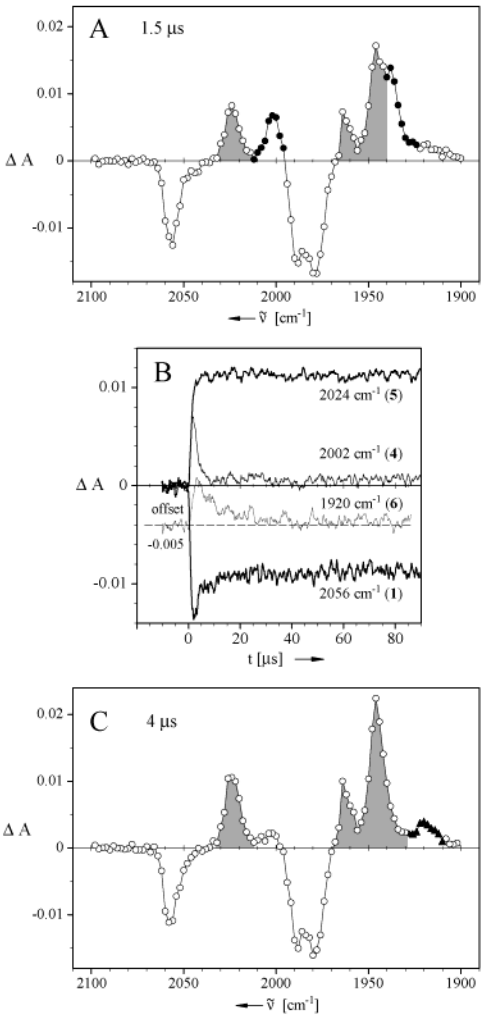

Figure 1. Flash photolysis (λ_{exc} = 308 nm) of $Fe(CO)_3(\eta^4$-1,3-bd) (**1**, 1.5 mM in cyclohexane solution) under CO atmosphere at ambient temperature with time-resolved IR detection in the 100 μs time range. (A) Transient ν(CO) difference spectrum recorded after 1.5 μs showing the depletion bands of **1** (2056, 1988, 1980 cm^{-1}) together with the absorptions of the photogenerated fragment $Fe(CO)_2(\eta^4$-1,3-bd)(solv) [**4** (●); 2002, 1938 cm^{-1}] and the species **5** (shaded areas; 2024, 1962, 1944 cm^{-1}), assigned (see text) as $Fe(CO)_3(\eta^4$-*s*-*trans*-1,3-bd). (B) Selected kinetic traces. (C) Difference spectrum recorded after 4 μs showing the depletion bands of **1** together with the absorptions of **5** (shaded areas) and $Fe(CO)_2(\eta^4$-1,3-bd)(H_2O) [**6** (▲); 1920 cm^{-1}].

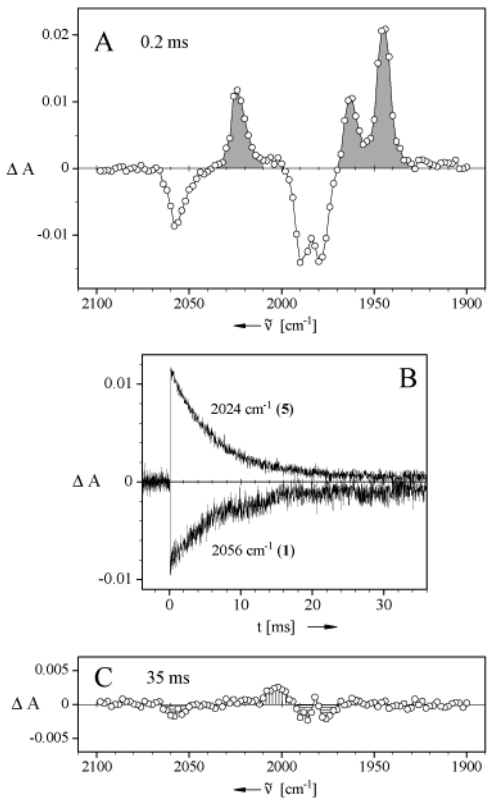

Figure 2. Flash photolysis (λ_{exc} = 308 nm) of $Fe(CO)_3(\eta^4$-1,3-bd) (**1**, 1.5 mM in cyclohexane solution) under CO atmosphere at ambient temperature with time-resolved IR detection in the 40 ms time range. (A) Transient ν(CO) difference spectrum recorded after 0.2 ms showing the depletion bands of **1** together with the absorptions of $Fe(CO)_3(\eta^4$-*s*-*trans*-1,3-bd) (**5**, shaded areas). (B) Decay of **5** (monitored at 2024 cm^{-1}) and recovery of **1** (monitored at 2056 cm^{-1}). (C) ν(CO) difference spectrum recorded after 35 ms showing residual depletion of **1** together with a weak absorption centered at 2004 cm^{-1} (hatched area), assigned (see text) as $Fe(CO)_4(\eta^2$-1,3-bd) (**2**).

photolysis of group 6 metal hexacarbonyls.[21,22] In support of this notion, the intensity of the 1920 cm^{-1} band is significantly increased upon deliberate contamination of the solution with water, which, moreover, slows down the decay to such an extent that it takes 60−70 μs until the absorbance returns to the baseline. Hence it seems that, despite all efforts made in the purification of the cyclohexane solvent, traces of moisture are still available for trapping the photogenerated fragment **4** in the form of an equilibrium with the species $Fe(CO)_2(\eta^4$-1,3-bd)(H_2O) (**6**), as suggested in Scheme 2. A second CO stretching mode of **6**, expected around 1980 cm^{-1}, is canceled due to overlap with the depleted absorption of **1** in this region.

The following discussion focuses on the assignment of the three prominent bands at 2024, 1962, and 1944 cm^{-1}, marked as shaded areas in Figure 1A and 1C. The same pattern was previously observed upon photolysis of **1** in low-temperature matrixes (2029, 1970, and 1953 cm^{-1} in Ar; 2023, 1963, and 1944 cm^{-1} in Xe)[16] and, at that time, was attributed to the coordinately unsaturated tricarbonyliron species $Fe(CO)_3(\eta^2$-1,3-bd) (**3**). However, this assignment does not seem consistent with its behavior in CO-saturated solution. By analogy with the very fast reaction of the dicarbonyl fragment **4** with CO, one would expect that the vacant coordination site of **3** is likewise rapidly occupied by carbon monoxide, which, in this case, would lead to the tetracarbonyl complex $Fe(CO)_4(\eta^2$-1,3-bd) (**2**). In striking contrast to this expectation, the three-band species survives virtually untouched from ca. 2 μs to 90 μs (as illustrated in Figure 1B by the ΔA trace recorded at 2024 cm^{-1}) and even beyond (0.2 ms, Figure 2A). It then decays gradually with concomitant and nearly complete recovery of **1** (Figure 2B), while the take-up of CO with formation of **2** is, at best, an insignificant side reaction (which for the sake of completeness is nevertheless included in

(21) Hermann, H.; Grevels, F.-W.; Henne, A.; Schaffner, K. *J. Phys. Chem.* **1982**, *86*, 5151−5154.
(22) Church, S. P.; Grevels, F.-W.; Hermann, H.; Schaffner, K. *Inorg. Chem.* **1985**, *24*, 418−422.

Table 1. Frequencies and Intensities of the CO Stretching Vibrations of $Fe(CO)_3(\eta^4$-*s*-*cis*-1,3-bd) (1), $Fe(CO)_4(\eta^2$-1,3-bd) (2), $Fe(CO)_3(\eta^2$-1,3-bd) (3), $Fe(CO)_3(\eta^4$-*s*-*trans*-1,3-bd) (5), $Fe(CO)_5$, $Fe(CO)_4$(solv), and $Fe(CO)_3$(solv)[i]

	frequency [cm^{-1}]		integrated intensity [$km \cdot mol^{-1}$][a]		
	exptl	calcd	exptl	calcd	ϵ [$L \cdot mol^{-1} \cdot cm^{-1}$]
1[b]	2054.8 (A′)	2044.0	274.1 (0.248)	475.2 (0.248)	5460
(C_s)	1988.5 (A′)	1992.8	462.4 (0.419)	816.4 (0.426)	8380
	1978.6 (A″)	1985.4	367.3 (0.333)	625.3 (0.326)	6510
2[b]	2082.5 (A_1)		102.7 (0.075)		2210
(C_{2v})[c]	2011.5 (A_1)		189.1 (0.138)		2550
	2003.6 (B_1)		595.6 (0.433)		11660
	1983.2 (B_2)		487.1 (0.354)		6840
3[d]		2036.6		561.4 (0.278)	
		1987.0		862.8 (0.427)	
		1980.7		596.3 (0.295)	
5[e]	2024	2023.6	(0.293)[f]/(0.217)[g]	555.8 (0.280)	
(C_1)	1962	1975.7	(0.210)[f]/(0.262)[g]	423.2 (0.213)	
	1944	1959.5	(0.496)[f]/(0.522)[g]	1009.0 (0.508)	
$Fe(CO)_5$[b]	2022.0 (A_2'')				9920
(D_{3h})	1999.0 (E′)				13220
$Fe(CO)_4 \cdot S$[h]	2084 (A_1)				
(C_{2v})	1986 (B_1)				
	1970 (A_1)				
	1950 (B_2)				
$Fe(CO)_3 \cdot S$[h]	1926 (E)				
(C_{3v})					

[a] Relative integrated intensities are given in parentheses. [b] Experimental data from FTIR spectra. [c] $Fe(CO)_4$ skeleton assumed to possess local C_{2v} symmetry. [d] Data calculated for singlet **3**; data for triplet **3** are listed in ref 52. [e] Experimental data from transient IR spectra recorded after flash photolysis of **1** (Figure 2A) and **2** (Figure 11A), respectively. [f] Data from Figure 2A. [g] Data from Figure 11A. [h] Experimental data from transient IR spectra recorded after flash photolysis of $Fe(CO)_5$ (Figure 9A); S = solvent cyclohexane. [i] Experimental and calculated data are taken from measurements in cyclohexane solution and from BP86 DFT calculations, respectively.

Scheme 2

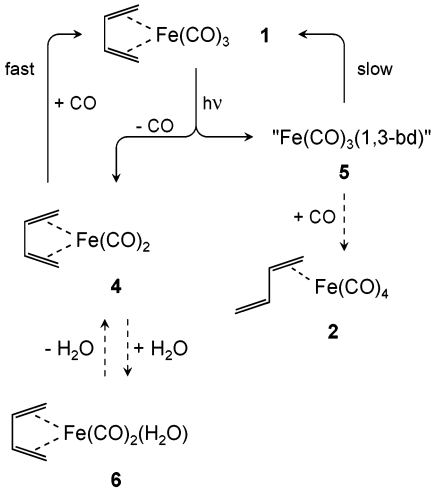

Scheme 2). This is evident from the difference spectrum recorded after 35 ms (Figure 2C), which exhibits no more than minor remnants of the depletion pattern of **1** along with a rather weak product absorption around 2004 cm^{-1}, attributable to the strongest of the four ν(CO) bands of **2** (cf. Table 1 for reference data).

Hence we conclude that we are actually dealing with a coordinately saturated isomer of **1**, a structure containing η^4-coordinated 1,3-butadiene in its *s*-*trans* conformation (**5**) being an appealing proposal. This coordination mode of a 1,3-diene has some well-documented precedents among early transition metal (η^4-diene)-metallocenes[23−27] and other 1,3-diene complexes of late transition metals in higher oxidation states,[28−34] but is a novelty in diene-substituted zerovalent metal carbonyls. The ν(CO) pattern of **5** (Figures 1C and 2A) bears some resemblance to that of trigonal-bipyramidal *fac*-$Fe(CO)_3(\eta^2$-ethene)(PR_3) complexes.[35] This leads us to suggest a similar coordination geometry for **5** with one C═C unit of the diene residing in an axial and the other one in an equatorial coordination site.

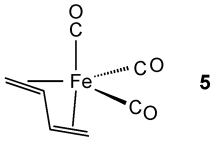

The ΔA traces recorded in the 40 ms time range show satisfactory fits to first-order kinetics, regardless of

(23) Erker, G.; Wicher, J.; Engel, K.; Rosenfeldt, F.; Dietrich, W.; Krüger, C. *J. Am. Chem. Soc.* **1980**, *102*, 6344−6346.

(24) Erker, G.; Wicher, J.; Engel, K.; Krüger, C. *Chem. Ber.* **1982**, *115*, 3300−3310.

(25) Kai, Y.; Kanehisa, N.; Miki, K.; Kasai, N.; Mashima, K.; Nagasuna, K.; Yasuda, H.; Nakamura, A. *J. Chem. Soc., Chem. Commun.* **1982**, 191−192.

(26) Erker, G.; Krüger, C.; Müller, G. *Adv. Organomet. Chem.* **1985**, *24*, 1−39.

(27) Yasuda, H.; Tatsumi, K.; Nakamura, A. *Acc. Chem. Res.* **1985**, *18*, 120−126.

(28) Hunter, A. D.; Legzdins, P.; Nurse, C. R.; Einstein, F. W. B.; Willis, A. C. *J. Am. Chem. Soc.* **1985**, *107*, 1791−1792.

(29) Hunter, A. D.; Legzdins, P.; Einstein, F. W. B.; Willis, A. C.; Bursten, B. E.; Gatter, M. G. *J. Am. Chem. Soc.* **1986**, *108*, 3843−3844.

(30) Christensen, N. J.; Hunter, A. D.; Legzdins, P. *Organometallics* **1989**, *8*, 930−940.

(31) Benyunes, S. A.; Green, M.; Grimshire, M. J. *Organometallics* **1989**, *8*, 2268−2270.

(32) Benyunes, S. A.; Day, J. P.; Green, M.; Al-Saadoon, A. W.; Waring, T. L. *Angew. Chem.* **1990**, *102*, 1505−1507; *Angew. Chem., Int. Ed. Engl.* **1990**, *29*, 1416−1417.

(33) Ernst, R. D.; Melendez, E.; Stahl, L.; Ziegler, M. L. *Organometallics* **1991**, *10*, 3635−3642.

(34) Benyunes, S. A.; Binelli, A.; Green, M.; Grimshire, M. J. *J. Chem. Soc., Dalton Trans.* **1991**, 895−904.

whether the decay of **5** or the recovery of depleted **1** is monitored, as exemplarily illustrated in Figure 2B. Variable-temperature measurements, carried out in a thermostated cuvette, yielded $k_{obs} = 76.4$ (± 4.6) s^{-1} at 24.6 °C (with 0.5 mM **1**), 76.9 (± 3.4) s^{-1} at 25.5 °C (with 1.5 mM **1**), 129 s^{-1} (± 4) at 30.3 °C (with 1.5 mM **1**), and 556 (± 24) s^{-1} at 46.0 °C (with 1.5 mM **1**). These data are average values from curve fittings at 18 or more different monitoring wavenumbers in each set of measurements. At any temperature, nearly complete recovery of **1** is observed; that is, the side reaction of **5** with CO with formation of **2** can be considered as negligible. The Arrhenius plot of the above rate constants is a straight line yielding $E_a = 17.9$ kcal·mol^{-1} ($A = 9.6 \times 10^{14}$ s^{-1}; $\Delta H^{\ddagger} = E_a - RT = 17.3$ kcal·mol^{-1}).[36] This activation barrier is of the same order of magnitude as the values reported for the *s-trans* → *s-cis* isomerization of $Cp_2Zr(\eta^4$-1,3-diene) complexes ($\Delta G^{\ddagger} = 18.2-22.7$ kcal·mol^{-1} at $t = -25$ to 10.5 °C),[23,24,26] thus providing further support for the assignment of **5** as $Fe(CO)_3(\eta^4$-*s-trans*-1,3-bd).

Density Functional Study of $Fe(CO)_3$(1,3-butadiene) Species with Varying Diene Dihedral Angles. In search of complementary information on the transient $Fe(CO)_3(\eta^4$-*s-trans*-1,3-butadiene) (**5**) and related species we examined this system by means of density functional theory (DFT)[37−39] methods, which have become useful tools for the study of molecular structures, transition states, and force fields of a wide variety of complexes including, for example, metal carbonyls.[40,41]

We first revisit $Fe(CO)_3(\eta^4$-*s-cis*-1,3-bd) (**1**), which was recently studied by Bühl and Thiel[41] with particular emphasis on the CO stretching frequencies in the context of rotational CO site exchange. Our results compare well with that study. The computed geometry of **1** (Figure 3), obtained without imposing symmetry restrictions, shows no significant deviations from the structure found in the crystal.[8] Satisfactory agreement between calculated and experimental data is also found for the CO stretching vibrational pattern of **1** (Table 1) with respect to both the frequencies and the relative intensities, while the absolute intensities show a systematic deviation by a factor of 1.7.

In light of this encouraging test, we are confident that the applied level of theory is sufficient to yield reliable information on isomeric species with different conformations of the 1,3-butadiene ligand. Before going into detail, we wish to premise that our study not only corroborates the proposed structure of the observed transient $Fe(CO)_3(\eta^4$-*s-trans*-1,3-bd) (**5**) but also hints at the existence of the coordinately unsaturated species $Fe(CO)_3(\eta^2$-1,3-bd) (**3**) in another minimum, albeit rather flat, on the potential energy surface of the $Fe(CO)_3$(1,3-bd) system.

In a series of partial geometry optimizations, the C10−C9−C8−C11 dihedral angle ϕ_d of the diene is varied, in steps of 20°, from 100° to ±180° and further to −100°,[42] with the C11═C8 double bond remaining attached to the metal. In each of these calculations,[43] the angle ϕ_d is kept fixed while all other coordinates are optimization parameters. The plot of the calculated energies versus ϕ_d (Figure 4) shows a well-pronounced minimum in the range 120−140°, while a nearly flat region is seen around −160°.

A full geometry optimization, in which the restriction of $\phi_d = 140°$ is released, leads to a structure that in essence shows the features proposed for the transient species $Fe(CO)_3(\eta^4$-*s-trans*-1,3-bd) (**5**). It resides in a minimum located 20.3 kcal·mol^{-1} above the parent $Fe(CO)_3(\eta^4$-*s-cis*-1,3-bd) (**1**) (Figure 5). This energy difference is smaller than previously predicted (1.3 eV = 30 kcal·mol^{-1})[27,44] on the basis of extended Hückel calculations, which, however, used merely a rough estimate of the geometry of **5**.

The computed structure of **5** (Figure 3) contains a *fac*-$Fe(CO)_3$ skeleton as part of a slightly distorted trigonal bipyramid with an angle of 123.0° between the two equatorial CO groups and with angles of 90.8° and 89.7° between the CO group in the axial position and the equatorial carbonyls. The remaining two coordination sites of **5**, one axial and one equatorial, are occupied by the C═C double bonds of the diene. These two vinyl units are significantly twisted away from coplanarity, as indicated by the computed C10−C9−C8−C11 dihedral angle of 129°. Note that similar characteristics of 1,3-diene ligands were experimentally found for the compounds $Cp_2Zr(\eta^4$-*s-trans*-1,4-diphenyl-1,3-butadiene),[25,27] $CpMo(NO)(\eta^4$-*s-trans*-2,5-dimethyl-2,4-hexadiene),[28] and $Ru(\eta^4$-*s-trans*-2,4-dimethyl-1,3-pentadiene)(acac),[33] which show torsion angles about the central C−C bond of ca. 126°, 124.8°, and 122.6°, respectively.[45] Regarding the carbon−carbon bond lengths, it is interesting to note that the alternation, present in free *s-trans*-1,3-butadiene (1.337 Å, C═C; 1.483 Å, C−C),[46] is still preserved in $Fe(CO)_3(\eta^4$-*s-trans*-1,3-bd) (**5**), al-

(35) Lindner, E.; Schauss, E.; Hiller, W.; Fawzi, R. *Chem. Ber.* **1985**, *118*, 3915−3931.

(36) With a barrier of this height, it should be possible to slow the thermal **5** → **1** rearrangement at low temperatures to such an extent that NMR spectroscopy can be employed for complementary characterization (we thank one reviewer for drawing our attention to this issue), by analogy with the study of a thermally labile carbonyliron complex, $HFe(CO)_3(\eta^3$-$C_3H_5)$, photogenerated by continuous irradiation of $Fe(CO)_4(\eta^2$-$C_3H_6)$ (Barnhart, T. M.; De Felippis, J.; McMahon, R. J. *Angew. Chem.* **1993**, *105*, 1134−1136; *Angew. Chem., Int. Ed. Engl.* **1993**, *32*, 1073−1074). Complex **5**, generated by continuous irradiation of **1** in 2-methylpentane solution at −120 °C, proved indeed sufficiently long-lived for detection by FTIR spectroscopy. However, the conversion of **1** does not exceed 1−2%, such that the concentration of **5** remains at a stationary level which is much too low for recording its NMR spectrum. It seems that the system is photoreversible, by analogy with previous observations made in low-temperature matrixes.[16]

(37) Koch, W.; Holthausen, M. C. *A Chemist's Guide to Density Functional Theory*; Wiley-VCH: Weinheim, 1999.

(38) Labanowski, J. K., Andzelm, J. W., Eds. *Density Functional Methods in Chemistry*; Springer: New York, 1991.

(39) Ziegler, T. *Chem. Rev.* **1991**, *91*, 651−667.

(40) Jonas, V.; Thiel, W. *J. Chem. Phys.* **1995**, *102*, 8474−8484.

(41) Bühl, M.; Thiel, W. *Inorg. Chem.* **1997**, *36*, 2922−2924.

(42) Recall that the two vinyl units of η^4-*s-cis*-coordinated 1,3-butadiene are bound to a metal with opposite enantiotopic faces, while the same enantiotopic faces are involved in the case of η^4-*s-trans*-coordinated 1,3-butadiene. The numbering of the diene carbon atoms chosen in Figure 3 for $Fe(CO)_3(\eta^4$-*s-cis*-1,3-bd) (**1**) involves the *R* configuration for C9 and the *S* configuration for C8. The vinyl unit containing C8 is kept attached to the metal when the C10−C9−C8−C11 dihedral angle is varied in the series of partial geometry optimizations performed in search of the structure of the η^4-*s-trans* isomer **5**. In consequence of this choice, the configuration of C9 is inverted from *R* to *S* on going from **1** to **5** and, moreover, the diene dihedral angle ϕ_d has a positive value in **5**.

(43) A spin multiplicity of 1 was chosen throughout, unless otherwise noted.

(44) Tatsumi, K.; Yasuda, H.; Nakamura, A. *Isr. J. Chem.* **1983**, *23*, 145−150.

(45) The geometry of the diene ligand in the zirconocene derivative $Cp_2Zr(\eta^4$-*s-trans*-1,3-butadiene)[23,24] remained ambiguous due to unusually high thermal parameters of the central carbon atoms.

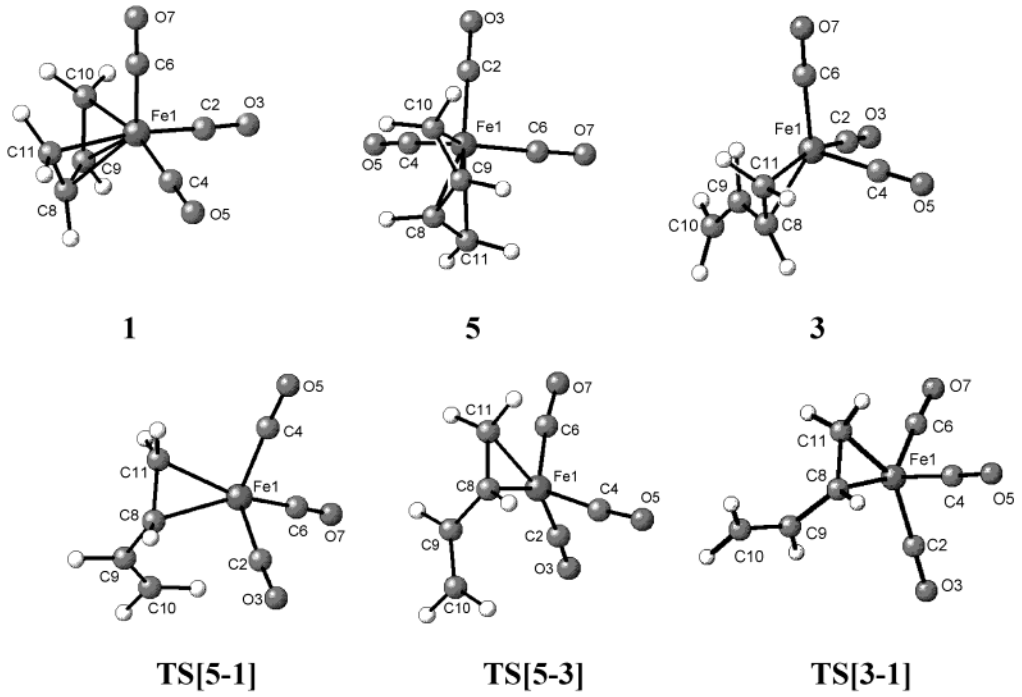

	1	TS[5-1]	5	TS[5-3]	3[a)]	TS[3-1]
dihedral angle [deg]:						
C10-C9-C8-C11	0.0 (0.0)	95.7	129.0	163.4	-150.1	-84.7
angles [deg]:						
C6-Fe1-C2	101.9 (102)	90.8	90.8	94.8	104.8	110.4
C6-Fe1-C4	101.9 (102)	91.0	123.0	117.5	101.3	96.4
C2-Fe1-C4	91.8 (93)	120.8	89.7	90.7	90.0	89.6
C11-C8-C9	117.4 (118)	121.4	117.9	116.9	115.6	121.0
C10-C9-C8	117.4 (118)	127.9	113.9	124.7	134.2	123.5
distances [Å]:						
Fe1-C11	2.126 (2.14±0.04)	2.072	2.262	2.155	2.109	2.035
Fe1-C8	2.078 (2.06±0.03)	2.107	2.063	2.038	2.035	2.050
Fe1-C9	2.078 (2.06±0.03)	3.011	2.057	2.416	2.158	2.926
Fe1-C10	2.126 (2.14±0.04)	3.274	2.221	3.158	3.385	4.213
C11-C8	1.436 (1.46±0.05)	1.422	1.408	1.418	1.435	1.436
C8-C9	1.426 (1.45±0.06)	1.497	1.461	1.470	1.444	1.505
C9-C10	1.436 (1.46±0.05)	1.345	1.407	1.364	1.358	1.346
energy [a.u.]	-620.112344	-620.053164	-620.078767	-620.064249	-620.064996	-620.046217
with ZPE correction	-620.000489	-619.944254	-619.968078	-619.954949	-619.956307	-619.938533
imag. freq. [cm^{-1}]		87.1·i		70.7·i		181.1·i

[a)] Data calculated for the triplet of **3** are given in ref. 52.

Figure 3. BP86 optimized geometries[42,43] of $Fe(CO)_3(\eta^4$-*s*-*cis*-1,3-bd) (**1**), the fragment $Fe(CO)_3(\eta^2$-*s*-*trans*-1,3-bd) (**3**), $Fe(CO)_3(\eta^4$-*s*-*trans*-1,3-bd) (**5**), and the transition states **TS[5−1]**, **TS[5−3]**, and **TS[3−1]** along with the respective energies and selected bond distances and angles. For comparison, data from the X-ray structure analysis[8] of **1** are given in parentheses.

though much less pronounced (1.407/1.408 Å, C═C; 1.461 Å, C−C). Recall that for the η^4-*s*-*cis* complex **1** nearly equal C═C and C−C distances are experimentally found (1.46 ± 0.05 Å, C═C; 1.45 ± 0.06 Å, C−C)[8] and computed (1.435 Å, C═C; 1.426 Å, C−C; see Figure 3). This is consistent with the notion[27] of more effective back-donation from the metal into the π_3* acceptor

(46) Sutton, E. L., Ed. *Tables of Interatomic Distances and Configuration in Molecules and Ions. Supplement 1956−1959*; The Chemical Society: London, 1965; Sect. B, M 109s.

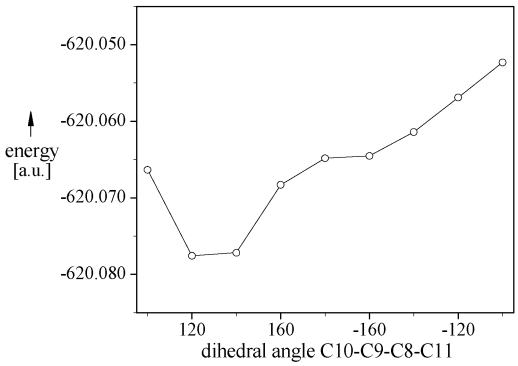

Figure 4. Energies of partially optimized geometries of $Fe(CO)_3$(1,3-bd) computed at the BP86 level of DFT with various C10−C9−C8−C11 dihedral angles ϕ_d of the diene ligand.[42]

orbital of the η^4-*s*-*cis*-coordinated 1,3-butadiene in **1** compared with the η^4-*s*-*trans*-coordinated 1,3-butadiene in **5**, which seems to be largely responsible for the energy difference between the two compounds.

A further minimum is found in the nearly flat region of the diagram shown in Figure 4. In this case, a full geometry optimization is started with the partially optimized structure obtained with $\phi_d = -160°$. The computed structure (Figure 3) shows a dihedral angle of $\phi_d = -150.1°$, and the Fe−C(diene) and the C═C distances indicate that only one vinyl group of the 1,3-butadiene ligand is bound to the $Fe(CO)_3$ unit; that is, we are dealing with the coordinately unsaturated species $Fe(CO)_3(\eta^2$-1,3-bd) (**3**). The minimum is located 7.4 kcal·mol^{-1} above $Fe(CO)_3(\eta^4$-*s*-*trans*-1,3-bd) (**5**) and 27.7 kcal·mol^{-1} above $Fe(CO)_3(\eta^4$-*s*-*cis*-1,3-bd) (**1**) (Figure 5).

Fragments of type $Fe(CO)_3(\eta^2$-olefin)[47,48] and $Fe(CO)_3(\eta^2$-diene)[49] have been suggested to possess a triplet ground state, by analogy with (naked) $Fe(CO)_4$.[50,51] Hence one might argue that the electronic ground state of **3** is also a triplet rather than a singlet, as tacitly assumed in the above treatment.[43] To address this point, a comparative calculation is performed for the triplet case.[52] The results place the triplet above the singlet, although the energy gap is as small as 0.3 kcal·mol^{-1} (0.5 kcal·mol^{-1} with ZPE) or 2.2 kcal·mol^{-1} (1.5 kcal·mol^{-1} with ZPE), depending on whether the calculation is performed at the unrestricted or restricted BP86 level of DFT. In either case, the η^2-coordinated 1,3-butadiene shows an almost coplanar arrangement of the two vinyl units ($\phi_d = 178.3°$ and 179.5°, respectively).

As regards the CO stretching vibrations, the observed transient product spectrum (Figure 2A, Table 1) is much better reproduced by the calculated pattern of $Fe(CO)_3(\eta^4$-*s*-*trans*-1,3-bd) (**5**) (Table 1) than by the calculated pattern of either singlet or triplet $Fe(CO)_3(\eta^2$-1,3-bd) (**3**).[52] This is particularly true for the relative intensities, as convincingly demonstrated in Figure 6, where all four spectra are displayed in schematic form. This further corroborates the assignment of the transient species as **5** rather than **3**.

Fragment **3** may nevertheless exist in an equilibrium with **5**, albeit in a concentration far too low for spectroscopic detection. We suppose that **3** is trapped by carbon monoxide, Scheme 3,[20] to yield the minor amount of $Fe(CO)_4(\eta^2$-1,3-bd) (**2**) observed as the side product of the thermal reconversion of photogenerated **5** into the stable η^4-*s*-*cis*-1,3-bd parent complex **1** in CO-saturated solution (vide supra, cf. Scheme 2).

One easily realizes that the **5** → **1** rearrangement involves rotation about the central C−C bond of the diene, either clockwise or counterclockwise, and requires the temporary detachment of one of the two vinyl units of the diene from the metal followed by reattachment with its opposite enantiotopic face.[42] The clockwise rotation proceeds via the species **3**, while the counterclockwise rotation directly converts **5** into **1**. For the respective transition states, designated as **TS[5−3]**, **TS[3−1]**, and **TS[5−1]** in Figure 5, one vibrational mode with an imaginary frequency is found (data listed in Figure 3) as requested for first-order saddle points on the potential energy surface.

The computed structures of **TS[5−1]** and **TS[3−1]** (Figure 3) show a nearly orthogonal orientation of the two vinyl units of the diene ligand relative to each other. The C10−C9−C8−C11 dihedral angle has a positive sign for **TS[5−1]** ($\phi_d = 95.7°$), whereas the sign is negative for **TS[3−1]** (−84.7°). It is the C11═C8 unit of **5** that remains coordinated in either case and experiences merely a moderate increase of its C═C distance. The carbon−carbon distance of the detached C10═C9 unit is substantially shortened and assumes a value that is almost identical with the C═C distance in free 1,3-butadiene[46] and with that of the uncoordinated vinyl group in **3** as well.

These transition states are rather close in energy, **TS[5−1]** and **TS[3−1]** being located 15.0 and 18.6 (7.4 +11.2) kcal·mol^{-1}, respectively, above **5** (Figure 5). Of the two alternative pathways, the direct conversion via **TS[5−1]** may be slightly favored over the two-step route

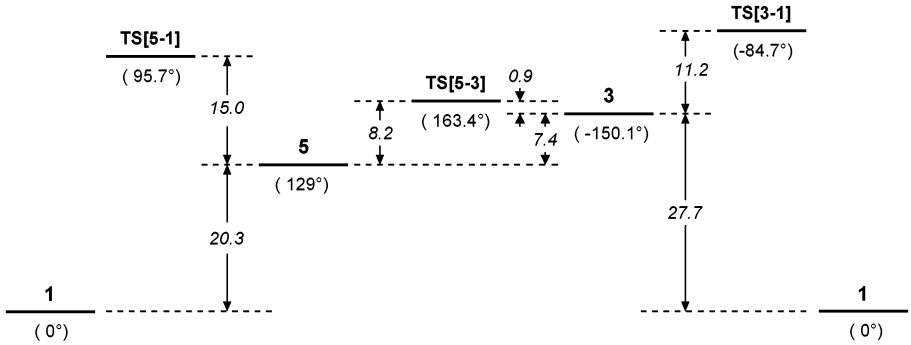

Figure 5. Energies [kcal·mol^{-1}] (with ZPE correction) and C10−C9−C8−C11 diene dihedral angles ϕ_d of $Fe(CO)_3(\eta^4$-*s*-*trans*-1,3-bd) (**5**), the fragment $Fe(CO)_3(\eta^2$-*s*-*trans*-1,3-bd) (**3**), and the transition states **TS[5−1], TS[5−3]**, and **TS[3−1]** in relation to $Fe(CO)_3(\eta^4$-*s*-*cis*-1,3-bd) (**1**), as computed at the BP86 level of DFT.

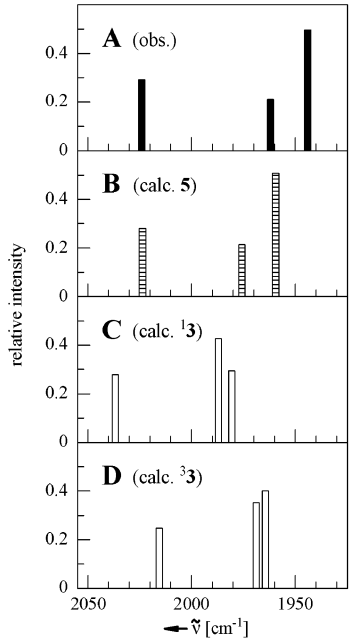

Figure 6. (A) Schematic representation of the observed transient ν(CO) product pattern attributed to Fe(CO)$_3$(η^4-*s-trans*-1,3-bd) (**5**) (Table 1; cf. Figure 2A). (B) Calculated ν(CO) spectrum of **5** (Table 1). (C) and (D): Calculated ν(CO) spectra of Fe(CO)$_3$(η^2-1,3-bd) (**3**, singlet and triplet, respectively; data from footnote 52).

Scheme 3

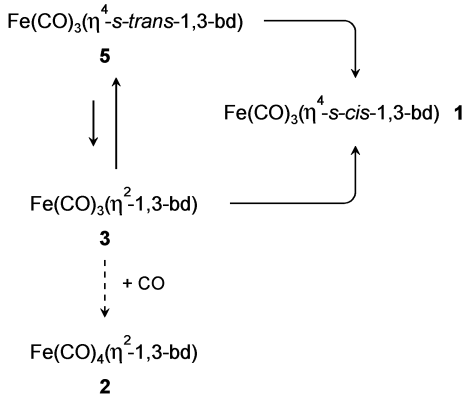

proceeding via **TS[5−3]**, **3**, and **TS[3−1]**. In either case, the computed barrier compares well with the experimentally determined activation energy for the **5** → **1** rearrangement (E_a = 17.9 kcal·mol^{-1}; $\Delta H^{\ddagger}$ = 17.3 kcal·mol^{-1}; vide supra), thus further substantiating the assignment of **5**.

Flash Photolysis of Fe(CO)$_5$ in the Presence of 1,3-Butadiene. Having accomplished the characterization of the transient photoproducts of Fe(CO)$_3$(η^4-*s-cis*-1,3-bd) (**1**), we now deal with the mechanistic aspects

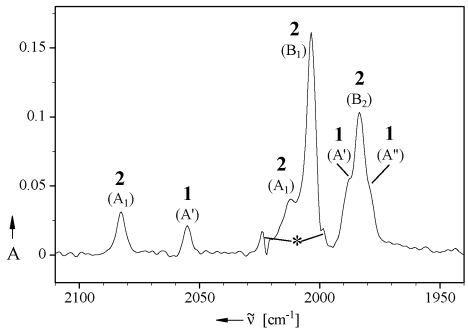

Figure 7. FTIR ν(CO) spectrum recorded after single-flash irradiation (λ_{exc} = 308 nm, 150 mJ incident flash energy) of Fe(CO)$_5$ (1.5 mM in cyclohexane containing 130 mM 1,3-butadiene) in an IR cell (d = 0.5 mm), illustrating the formation of Fe(CO)$_3$(η^4-1,3-bd) (**1**) and Fe(CO)$_4$(η^2-1,3-bd) (**2**) (for frequency data see Table 1) in 1:4 ratio. Note that the absorptions associated with unphotolyzed Fe(CO)$_5$ (78%) are removed by computer-assisted subtraction; small artifacts arising from this treatment are marked by the asterisk.

of its photochemical synthesis from Fe(CO)$_5$ and 1,3-butadiene, thought to involve the monosubstituted Fe(CO)$_4$(η^2-1,3-bd) (**2**) as an intermediate product (Scheme 1).[5]

Using FTIR spectroscopy for monitoring the progress of this conversion, we note that complex **2** does not accumulate under continuous irradiation (λ_{exc} = 313 nm). It rather remains at a relatively low level of concentration, thus indicating that the secondary, intramolecular CO photosubstitution leading to **1** occurs with high efficiency.[53]

The result of single-flash irradiation under similar conditions (λ_{exc} = 308 nm; 1.5 mM Fe(CO)$_5$; 130 mM 1,3-butadiene in cyclohexane solution under argon atmosphere) is shown in Figure 7. The product spectrum is dominated by the well-resolved four-band ν(CO) pattern of the tetracarbonyl complex **2**, which, however, is accompanied by additional absorptions indicative of the tricarbonyl complex **1** (frequencies listed in Table 1). This means that, surprisingly enough, a single-photon route from Fe(CO)$_5$ to **1** is operative in addition to the previously suggested (Scheme 1) two-step sequence

$$\mathrm{Fe(CO)_5} \xrightarrow{h\nu} \mathbf{2} \xrightarrow{h\nu} \mathbf{1}$$

This additional route accounts for not less than 20% of the product mixture.

(47) Barnhart, T. M.; Fenske, R. F.; McMahon, R. J. *Inorg. Chem.* **1992**, *31*, 2679−2681.
(48) Barnhart, T. M.; McMahon, R. J. *J. Am. Chem. Soc.* **1992**, *114*, 5434−5435.
(49) Gravelle, S. J.; van de Burgt, L. J.; Weitz, E. *J. Phys. Chem.* **1993**, *97*, 5272−5283.
(50) Poliakoff, M.; Weitz, E. *Acc. Chem. Res.* **1987**, *20*, 408−414, and references therein.
(51) Poliakoff, M.; Turner, J. J. *Angew. Chem.* **2001**, *113*, 2889−2892; *Angew. Chem., Int. Ed.* **2001**, *40*, 2809−2812, and references therein.

(52) We thank one reviewer for drawing our attention to this issue. The geometry optimization for the triplet was started with the structure of singlet **3** shown in Figure 3. If performed at the unrestricted BP86 level of DFT (the application of which seems justified by an S^2 expectation value of 2.03), it yielded an energy of −620.064492 au (−619.957052 au with ZPE correction). All frequencies are real. CO stretching vibrational frequencies and intensities: 2015.5 cm^{-1} (523.1 km·mol^{-1}; 0.248 rel), 1968.9 (741.1; 0.352), and 1964.4 (842.9; 0.400). Selected angles [deg] and bond distances [Å] (for the numbering scheme see Figure 3): 178.3 (C10−C9−C8−C11), 100.3 (C6−Fe1−C2), 98.2 (C6−Fe1−C4), 97.0 (C2−Fe1−C4), 123.7 (C11−C8−C9), 124.1 (C10−C9−C8); 2.169 (Fe1−C11), 2.168 (Fe1−C8), 2.680 (Fe1−C9), 3.611 (Fe1−C10), 1.399 (C11−C8), 1.457 (C8−C9), 1.366 (C9−C10). The alternative calculation at the restricted BP86 level of DFT yielded an energy of −620.061484 au (−619.953931 au with ZPE correction). All frequencies are real. CO stretching frequencies and intensities: 2014.9 cm^{-1} (524.8 km·mol^{-1}; 0.249 rel), 1969.0 (729.5; 0.346), and 1964.8 (854.9; 0.405). Selected angles [deg] and bond distances [Å]: 179.5 (C10−C9−C8−C11), 100.2 (C6−Fe1−C2), 98.2 (C6−Fe1−C4), 97.0 (C2−Fe1−C4), 123.8 (C11−C8−C9), 124.1 (C10−C9−C8); 2.170 (Fe1−C11), 2.174 (Fe1−C8), 2.719 (Fe1−C9), 3.655 (Fe1−C10), 1.398 (C11−C8), 1.459 (C8−C9), 1.363 (C9−C10).

Scheme 4

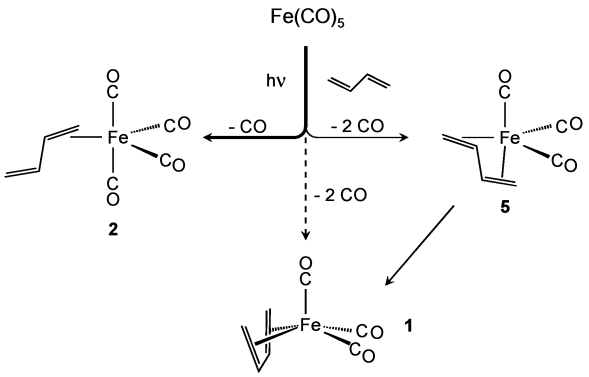

More detailed information on this route is gathered from studies employing flash photolysis in combination with time-resolved IR spectroscopy, which reveal that the novel isomer of **1**, $Fe(CO)_3(\eta^4$-*s*-*trans*-1,3-bd) (**5**), is involved as a transient species, Scheme 4.[20] The difference spectrum displayed in Figure 8A illustrates the situation after 1.5 μs. It shows the depletion bands of $Fe(CO)_5$ along with a product ν(CO) pattern which is dominated by the absorptions associated with the main product, $Fe(CO)_4(\eta^2$-1,3-bd) (**2**). Note that the strongest ν(CO) band of **2** (B_1), expected at 2003.6 cm^{-1} (Table 1), appears slightly shifted at 2006 cm^{-1} and with lower intensity than in Figure 7. We explain this apparent misrepresentation by taking into account the lower spectral resolution of the time-resolved IR instrumentation (7−8 vs 2 cm^{-1} of the FTIR spectrometer). This gives rise to some foot-and-tail overlap with the depleted E′ band of $Fe(CO)_5$ in close proximity (1999.0 cm^{-1}, Table 1) and, hence, causes noticeable mutual cancellation.

The two product absorptions at lower frequencies, rendered prominent as shaded areas in Figure 8A, are readily attributed to $Fe(CO)_3(\eta^4$-*s*-*trans*-1,3-bd) (**5**) by comparison with the complete ν(CO) transient spectrum of **5** observed upon flash photolysis of **1** (Figures 1C and 2A, Table 1). The third band of **5**, expected at 2024 cm^{-1}, is obscured by the depleted A_2'' absorption of $Fe(CO)_5$ near this position (2022.0 cm^{-1}, Table 1). At this early time (1.5 μs), **1** is present in rather small concentration. Only the high-frequency A′ ν(CO) band of **1** is just barely discernible at 2056 cm^{-1}, while the other two ν(CO) modes of this complex (A′ and A″, expected at 1988.5 and 1978.6 cm^{-1}, see Table 1) are masked by the much stronger B_2 absorption of **2** in the center of this region (1983.2 cm^{-1}, Table 1).

The subsequently occurring *s*-*trans* → *s*-*cis* rearrangement of the η^4-coordinated butadiene ligand at the $Fe(CO)_3$ unit, **5** → **1** (Scheme 4), is evident from the spectral changes monitored within a period of about 20 ms, which ultimately lead to the difference spectrum shown in Figure 8D. The gradual disappearance of **5** and the concomitant formation of **1** are exemplarily illustrated by the ΔA traces displayed in Figure 8B and 8C, respectively. Note the additional depletion at 2024 cm^{-1}, which confirms that the missing third band of **5**

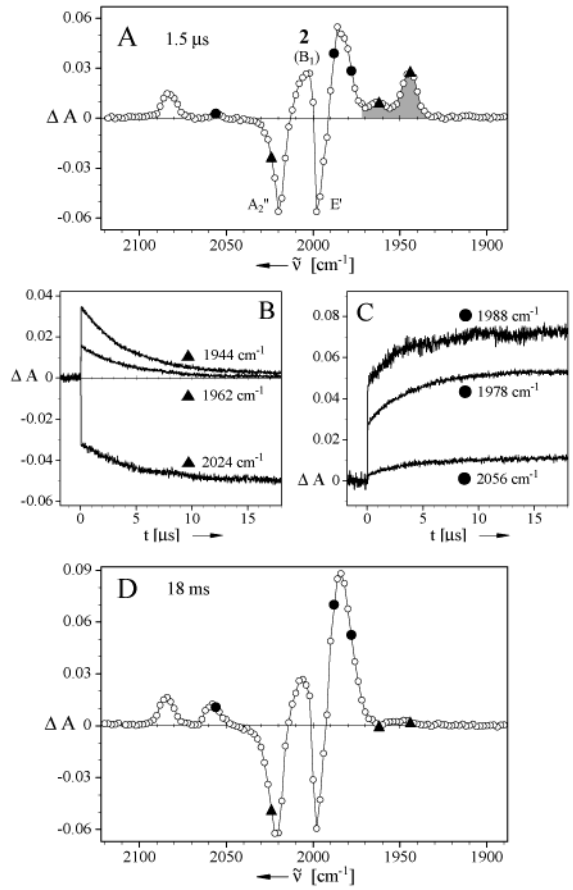

Figure 8. Flash photolysis (λ_{exc} = 308 nm) of $Fe(CO)_5$ (1.5 mM, in cyclohexane solution containing 130 mM 1,3-butadiene) under argon atmosphere at 25 °C. (A) Transient ν(CO) difference spectrum recorded after 1.5 μs showing the depletion bands of $Fe(CO)_5$ (2020, 1998 cm^{-1}) and the absorptions of photogenerated $Fe(CO)_4(\eta^2$-1,3-bd) (**2**) (2084, 2006, 1984 cm^{-1}) and $Fe(CO)_3(\eta^4$-*s*-*trans*-1,3-bd) (**5**) (1962, 1944 cm^{-1}; shaded area) along with a weak feature at 2056 cm^{-1} attributed to $Fe(CO)_3(\eta^4$-*s*-*cis*-1,3-bd) (**1**). (B) Decay of **5** monitored at the band positions listed in Table 1 and marked in spectra A and D by a solid triangle (▲). (C) Growth of **1** monitored at the band positions listed in Table 1 and marked in spectra A and D by a solid circle (●). (D) Spectrum recorded after 18 ms.

is indeed located at this position. The concentration of the main product **2** does not change during this period, as indicated by the constancy of ΔA at 2084 and 2006 cm^{-1}. The apparent increase of absorbance around the position of the B_2 ν(CO) band of **2** at 1984 cm^{-1} just reflects the growth of the closely spaced absorptions of **1** at 1988 and 1978 cm^{-1} (Figure 8C).

The absorbance changes recorded at a wide range of monitoring wavenumbers, including those displayed in Figure 8B and 8C, invariably show satisfactory fits to first-order kinetics, yielding an average value of k_{obs} = 250 (±24) s^{-1}. Comparative measurements under CO atmosphere instead of argon yield almost the same rate constant within the margins of error, k_{obs} = 274 (±18) s^{-1}. In other words, the presence of added CO (9.2 mM in CO-saturated cyclohexane)[54] has no noticeable influence on the decay of **5**. It does nevertheless change the

(53) An investigation into the gradual conversion of $Fe(CO)_5$ into $Fe(CO)_3(\eta^4$-*s*-*cis*-1,3-bd) (**1**) under continuous irradiation, aiming at the determination of quantum yields for the individual steps at various wavelengths, is in progress and will be published in a forthcoming paper.

(54) Wilhelm, E.; Battino, R. *J. Chem. Thermodyn.* **1973**, *5*, 117−120.

Scheme 5

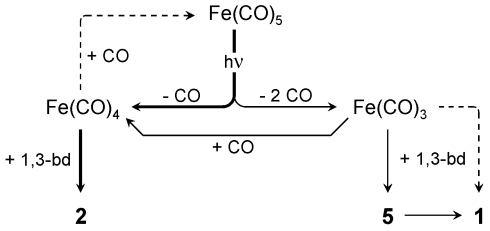

initial product distribution in a sense that it reduces the amount of the tricarbonyliron complex **5** in proportion to the main product **2** by a factor of about 0.6−0.7. Somewhat puzzling is the much higher velocity of the **5** → **1** rearrangement in comparison with the data ($k_{obs} \approx 77\ s^{-1}$) evaluated from those experiments where **5** was generated by photoisomerization of **1** in CO-saturated solution at nearly the same temperature (about 25 °C). This large acceleration (by a factor of 3.5) is certainly due to the presence of added 1,3-butadiene in high concentration, though we are not yet in a position to present a well-founded interpretation of this effect.[55]

The simplest way to rationalize the single-photon route from $Fe(CO)_5$ to the $Fe(CO)_3(\eta^4$-1,3-bd) complexes **5** and **1** would be to invoke the $Fe(CO)_3$(solv) as a directly photogenerated species, Scheme 5.[18,20] This would also explain the aforementioned influence of added CO on the initial product ratio, since competitive capturing of $Fe(CO)_3$(solv) by carbon monoxide on one hand and 1,3-butadiene on the other should ultimately favor the formation of the main product **2** at the expense of **5** (and **1**).

Photofragmentation of $Fe(CO)_5$ in the Absence of 1,3-Butadiene. We are aware that the above proposal conflicts with the conventional belief that multiple CO dissociation as a single-photon reaction of $Fe(CO)_5$ does not occur in condensed media,[50,56−58] although it has been observed in the gas phase.[59−61] Therefore, we set out to reexamine the flash photolysis of $Fe(CO)_5$ in hydrocarbon solution at ambient temperature, where $Fe(CO)_4$(solv) has been detected by means of time-resolved IR spectroscopy in the milli- and microsecond time range.[57,58] In the following we concentrate on the flash photolysis of $Fe(CO)_5$ in CO-saturated cyclohexane solution. Observations made in comparative experiments under argon atmosphere are nevertheless briefly mentioned, if relevant to the discussion.

The transient IR difference spectrum displayed in Figure 9A is recorded at a very early time (0.4 μs), shorter than the full response time of our detection system. It shows the depleted ν(CO) absorptions of $Fe(CO)_5$ along with a product spectrum that is dominated by the four-band pattern of the $Fe(CO)_4$(solv) fragment[58] (C_{2v} symmetry; 2 A_1, B_1, and B_2 ν(CO) modes). The frequencies of the latter species, as well as the relative intensities, are in good agreement with the data reported for the closely related (singlet) $Fe(CO)_4(CH_4)$, photogenerated from $Fe(CO)_5$ in a low-temperature methane matrix.[56]

In addition, a product band of moderate intensity, marked as a shaded area, is observed at 1926 cm^{-1}. This frequency is not far from the position of the E ν(CO) mode of the $Fe(CO)_3$ fragment in a methane matrix (1930.4 cm^{-1}),[56,62] such that the assignment to the species $Fe(CO)_3$(solv) is justified. The much weaker A_1 ν(CO) mode of this species, expected around 2036 cm^{-1} (2040.1 cm^{-1} in solid methane),[56,62] is just barely discernible at this wavenumber. This doubly unsaturated fragment decays very rapidly. As illustrated by the inset in Figure 9A, the absorption band at 1926 cm^{-1} has largely vanished within <1 μs, i.e., before the detection system has fully responded. It is no longer observable in the difference spectrum recorded after 1.2 μs (Figure 9B), which shows the well-developed ν(CO) pattern of $Fe(CO)_4$(solv).

At this time, the absorption at 2036 cm^{-1} has grown significantly, but is of course no longer attributable to the $Fe(CO)_3$(solv) fragment. Rather, it can be assigned to the unbridged form of the dinuclear species $Fe_2(CO)_8$, supposed to originate from the reaction of $Fe(CO)_3$(solv) with unphotolyzed $Fe(CO)_5$, Scheme 6,[18] by analogy with related findings in gas phase experiments.[61] The assignment is based on comparison with literature data available from low-temperature matrix studies, according to which the unbridged $Fe_2(CO)_8$[63,64] species exhibits two prominent bands at 2038 and 2006 cm^{-1} (in a CO-doped argon matrix). Although the latter position in our spectrum is obscured by the depleted E′ ν(CO) mode of $Fe(CO)_5$, this does not completely prevent the observation of an overlaid transient absorption centered at 2004 cm^{-1}, the growth and decay of which parallel the absorbance changes at 2036 cm^{-1} (Figure 9E). We assume that a certain amount of $Fe(CO)_3$(solv) is concomitantly trapped by CO with formation of additional $Fe(CO)_4$(solv). Unfortunately, we are not in a position to present direct spectroscopic evidence of the occurrence of this latter process, since it takes place within the response period of our instrumentation, during which the ν(CO) absorption signals of $Fe(CO)_4$(solv) continue to grow anyhow. However, the above assumption seems nevertheless justified, since in the absence of added CO it takes much longer (10−15 μs) until the absorption band of $Fe(CO)_3$(solv) at 1926 cm^{-1} has completely disappeared.

The fragment $Fe(CO)_4$(solv) vanishes with $k_{obs} \approx 2.7 \times 10^5\ s^{-1}$, as evaluated from the Δ*A* trace at 1986 cm^{-1} (inset in Figure 9B). A substantial amount, if not the predominant portion (vide infra), reacts with $Fe(CO)_5$ to form the dinuclear product $Fe_2(CO)_9$,[65] Scheme 6. This is evident from the ν(CO) bands emerging at 2056 cm^{-1} (barely discernible already after 1.2 μs, Figure 9B), in

(55) The apparent influence of various added trapping agents L, including both strongly binding ligands and weakly bound stand-in ligands, on the decay kinetics of photogenerated **5** is currently under investigation, a functional relationship of the type $k_{obs} = k_{iso}(1 + [L]) + k_L[L]$ being used as a working hypothesis.

(56) Poliakoff, M.; Turner, J. J. *J. Chem. Soc., Dalton Trans.* **1973**, 2276−2285.
(57) Church, S. P.; Grevels, F.-W.; Hermann, H.; Kelly, J. M.; Klotzbücher, W. E.; Schaffner, K. *J. Chem. Soc., Chem. Commun.* **1985**, 594−596.
(58) Grevels, F.-W. In *Photoprocesses in Transition Metal Complexes, Biosystems and other Molecules. Experiments and Theory*; Kochanski, E., Ed..; Kluwer: Dordrecht, 1992; pp 141−171.
(59) Yardley, J. T.; Gitlin, B.; Nathanson, G.; Rosan, A. M. *J. Chem. Phys.* **1981**, *74*, 370−378.
(60) Seder, T. A.; Ouderkirk, A. J.; Weitz, E. *J. Chem. Phys.* **1986**, *85*, 1977−1986.
(61) Ryther, R. J.; Weitz, E. *J. Phys. Chem.* **1991**, *95*, 9841−9852.
(62) Poliakoff, M. *J. Chem. Soc., Dalton Trans.* **1974**, 210−212.
(63) Poliakoff, M.; Turner, J. J. *J. Chem. Soc. (A)* **1971**, 2403−2410.
(64) Fletcher, S. C.; Poliakoff, M.; Turner, J. J. *Inorg. Chem.* **1986**, *25*, 3597−3604.

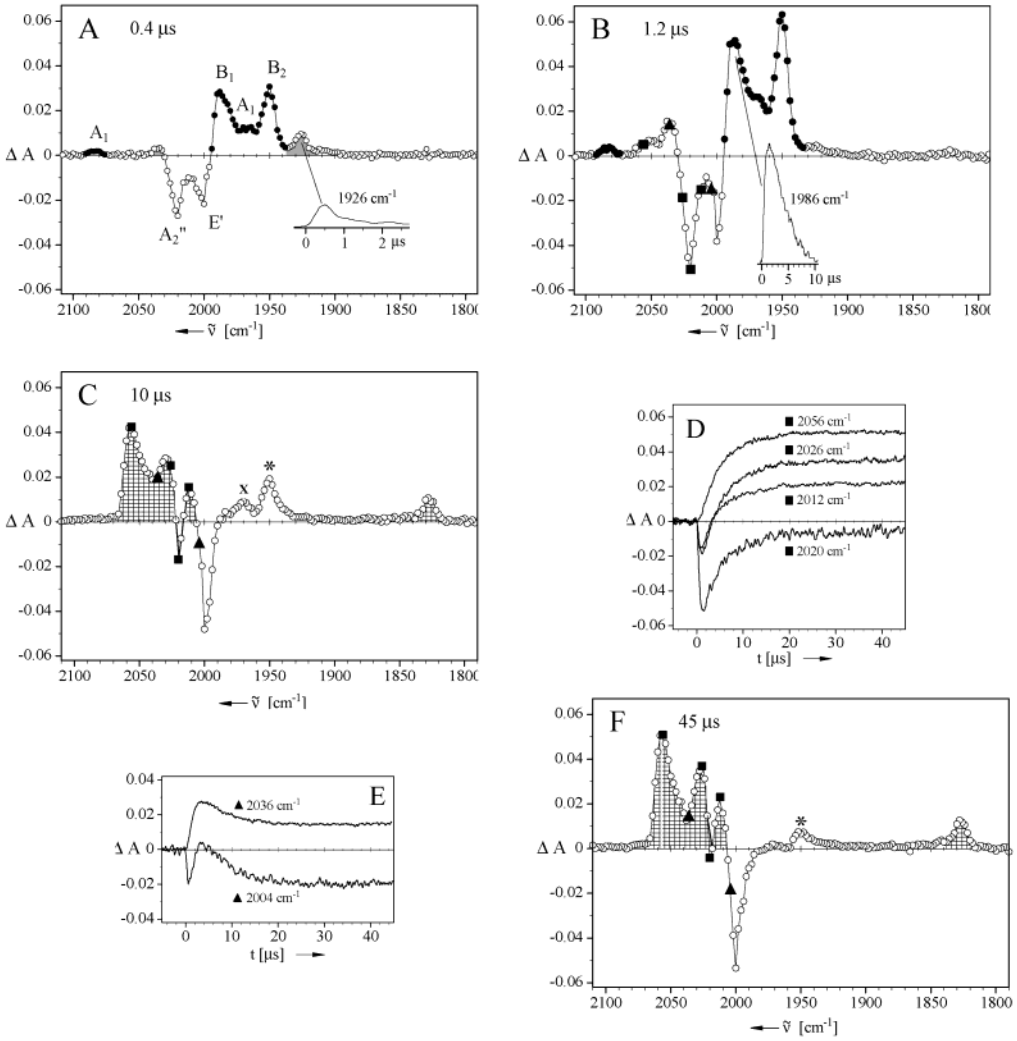

Figure 9. Flash photolysis ($\lambda_{exc} = 308$ nm) of $Fe(CO)_5$ (2 mM, in CO-saturated cyclohexane solution) at 25 °C. (A) Transient ν(CO) difference spectrum recorded after 0.4 μs showing the depletion bands of $Fe(CO)_5$ [2020 (A_2''), 1998 cm^{-1} (E′)] and the absorptions of the photogenerated fragments $Fe(CO)_4$(solv) [2084 (A_1), 1986 (B_1), 1970 (A_1), 1950 (B_2) cm^{-1}; ●)] and $Fe(CO)_3$(solv) [1926 (E) cm^{-1}; shaded area]. (B) Spectrum recorded after 1.2 μs showing the fully developed ν(CO) pattern of $Fe(CO)_4$(solv) (●) along with weak absorptions at 2056 and 2036 cm^{-1}, attributed (see text) to $Fe_2(CO)_9$ and $Fe_2(CO)_8$. (C) Spectrum recorded after 10 μs showing the ν(CO) pattern of $Fe_2(CO)_9$ (hatched area, for details see text) along with two residual absorptions at 1950 cm^{-1} [(*), assigned to $Fe(CO)_4(H_2O)$] and 1970 cm^{-1} (associated with an unidentified species X). (D) Growth of $Fe_2(CO)_9$ monitored at the positions marked in spectra B, C, F by a solid square (■). (E) Growth and decay of $Fe_2(CO)_8$ monitored at the positions marked in spectra B, C, F by a solid triangle (▲). (F) Spectrum recorded after 45 μs showing the ν(CO) pattern of $Fe_2(CO)_9$ (hatched area) along with the residual absorption at 1950 cm^{-1} [(*), assigned to $Fe(CO)_4(H_2O)$].

Scheme 6

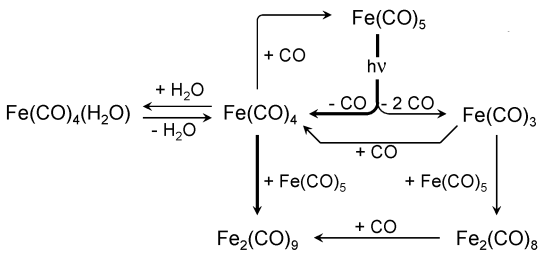

the 2030−2012 cm^{-1} region, and at 1826 cm^{-1}, which are rendered prominent as hatched areas in the spectrum recorded after 10 μs (Figure 9C). This pattern closely resembles the absorptions observed for $Fe_2(CO)_9$ under low-temperature matrix isolation conditions[63] (2064, 2037, and 1847.4 cm^{-1}; in a CO-doped argon matrix),[64] allowing for some shifts in frequency arising from the difference in temperature and media.[66]

Trapping of $Fe(CO)_4$(solv) by the added carbon monoxide with re-formation of $Fe(CO)_5$ is included in Scheme 6 as a competing process.[67] A reasonable esti-

(65) Recall that the photochemical conversion of $Fe(CO)_5$ into $Fe_2(CO)_9$, discovered a century ago as the first light-induced reaction in carbonylmetal chemistry, is a very efficient process providing high-yield access to $Fe_2(CO)_9$ on a preparative scale: (a) Mond, L.; Langer, C. *J. Chem. Soc., London* **1891**, *59*, 1090−1093. (b) Dewar, J.; Jones, H. O. *Proc. R. Soc., London (A)* **1905**, *76*, 558−577. (c) Speyer, E.; Wolf, H. *Chem. Ber.* **1927**, *60*, 1424−1425. (d) Brauer, G., Ed. *Handbuch der Präparativen Anorganischen Chemie*, 3rd ed.; Enke: Stuttgart, Germany, 1981; Vol. 3, pp 1827−1828.

(66) It is unfortunate that, due to the insolubility of $Fe_2(CO)_9$, data from spectra in solution are not available. The ν(CO) pattern of $Fe_2(CO)_9$ embedded in a potassium iodide pellet differs somewhat from the low-temperature matrix data with respect to the frequencies (2082, 2019, and 1829 cm^{-1}) and to the relative intensities as well: Cotton, F. A.; Liehr, A. D.; Wilkinson, G. *J. Inorg. Nucl. Chem.* **1955**, *1*, 175−186.

mate of the branching ratio of these two reaction channels of $Fe(CO)_4$(solv) is obtained by using complementary data from comparative measurements in the absence of added CO. Taking into account that under argon atmosphere the decay of $Fe(CO)_4$(solv) occurs with $k_{obs} \approx 1.8 \times 10^5\ s^{-1}$, we conclude that in CO-saturated solution ($k_{obs} \approx 2.7 \times 10^5\ s^{-1}$) only one-third of $Fe(CO)_4$(solv) is trapped by CO to re-form the parent $Fe(CO)_5$, while two-thirds react with $Fe(CO)_5$ to yield $Fe_2(CO)_9$, although CO is present in higher concentration (9.2 mM)[54] than $Fe(CO)_5$ (2 mM). This means that the reaction of $Fe(CO)_4$(solv) with $Fe(CO)_5$ ($k_{Fe(CO)5} \approx 9 \times 10^7\ L{\cdot}mol^{-1}{\cdot}s^{-1}$) is faster than the reaction with CO ($k_{CO} \approx 10^7\ L{\cdot}mol^{-1}{\cdot}s^{-1}$) by about 1 order of magnitude. It is interesting to note that this ratio has also been found in the gas phase,[61] where the reaction of photogenerated $Fe(CO)_4$ with the parent $Fe(CO)_5$ occurs with $k_{Fe(CO)5} = 5.2 \times 10^{-13}\ cm^3{\cdot}molecule^{-1}{\cdot}s^{-1}$, while trapping by added CO takes place with $k_{CO} = 5.2 \times 10^{-14}\ cm^3{\cdot}molecule^{-1}{\cdot}s^{-1}$.

The growth of $Fe_2(CO)_9$, exemplarily illustrated by the ΔA traces displayed in Figure 9D, is not terminated by the time (10 μs) when $Fe(CO)_4$(solv) has completely vanished. It rather proceeds further, though by irregular kinetics, thus hinting at other route(s) leading to $Fe_2(CO)_9$ as the ultimate product. The most obvious one involves the species $Fe_2(CO)_8$, which is converted into $Fe_2(CO)_9$ by taking up CO from the solution,[68] Scheme 6. This reaction occurs with $k_{obs} \approx 1.6 \times 10^5\ s^{-1}$, as evaluated from the decay of the ΔA traces recorded at 2036 and 2004 cm^{-1} (Figure 9E).

As shown in Figure 9C, the decay of $Fe(CO)_4$(solv) in CO-saturated solution leaves behind two residual absorptions at 1970 (×) and 1950 cm^{-1} (*), which before were masked by the strong absorptions of $Fe(CO)_4$(solv) at these positions. The first one has not yet been identified, whereas the second one (which is still observable after 45 μs, Figure 9F) is assigned to the species $Fe(CO)_4(H_2O)$, formed from $Fe(CO)_4$(solv) by reaction with apparently unavoidable traces of moisture.

This assignment rests on a comparative experiment carried out in water-saturated cyclohexane (0.01% ≙ 5.5 mM;[69] 3 mM[70]). The transient IR ν(CO) difference spectra recorded shortly after the flash photolysis of $Fe(CO)_5$ (Figure 10A) in essence still show the four-band product pattern of $Fe(CO)_4$(solv). However, at this stage already we note that the relative intensities of the B_1 and B_2 modes differ slightly from the picture familiar from measurements in rigorously dried solvent (Figure 9A and 9B). On going from 1.2 μs (spectrum displayed with closed circles, ●) to 2.0 μs (spectrum displayed with open circles, ○), the intensity at 1950 cm^{-1} increases noticeably at the expense of the absorption at 1986 cm^{-1}. The latter vanishes completely within 10 μs, whereas the former persists for a much longer time.

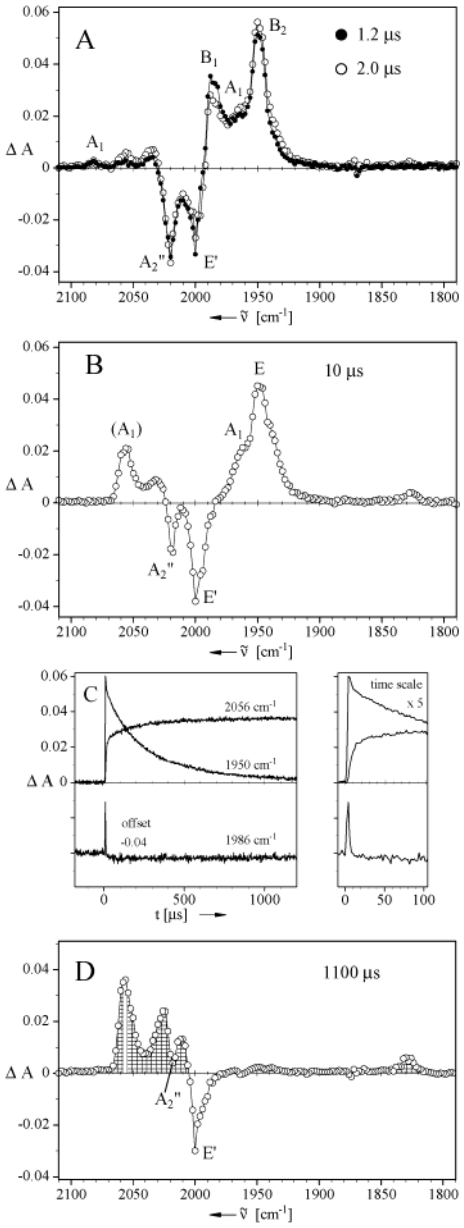

Figure 10. Flash photolysis ($\lambda_{exc} = 308$ nm) of $Fe(CO)_5$ (2 mM, in water-saturated cyclohexane solution) under CO atmosphere at 25 °C. (A) Transient ν(CO) difference spectra recorded after 1.2 μs (●) and 2.0 μs (○) showing the depletion bands of $Fe(CO)_5$ [2020 (A_2''), 1998 (E′) cm^{-1}] and the absorptions of photogenerated $Fe(CO)_4$(solv) [2084 (A_1), 1986 (B_1), 1970 (A_1), 1950 (B_2) cm^{-1}]. (B) Spectrum recorded after 10 μs showing product absorptions attributed to $Fe(CO)_4(H_2O)$ (2 A_1, E) and $Fe_2(CO)_9$ along with the depleted bands of $Fe(CO)_5$. (C) Decay of $Fe(CO)_4$(solv) and $Fe(CO)_4(H_2O)$ (monitored at 1986 and 1950 cm^{-1}) and growth of $Fe_2(CO)_9$ (monitored at 2056 cm^{-1}). (D) Spectrum recorded after 1100 μs showing the ν(CO) pattern of $Fe_2(CO)_9$ (hatched area) along with the depleted bands of $Fe(CO)_5$.

The spectrum recorded after 10 μs (Figure 10B) is dominated by the strong band at 1950 cm^{-1}, which exhibits a distinct shoulder at the high-frequency side (1964 cm^{-1}). In addition, three other absorptions have grown in at 2056, 2032, and 1826 cm^{-1}, which are

(67) Recall that the photoinduced exchange of CO for isotopically labeled carbon monoxide is a well-known reaction of $Fe(CO)_5$: (a) Noack, K.; Ruch, M. *J. Organomet. Chem.* **1969**, *17*, 309−322. (b) Bor, G. *Inorg. Chim. Acta* **1969**, *3*, 191−195.

(68) Under neat argon atmosphere, where merely the photodissociated carbon monoxide is available, this additional formation of $Fe_2(CO)_9$ seems negligible. What occurs instead is the growth of a strong absorption in the 2050−2040 cm^{-1} region, which fills the gap between the apparent maxima of $Fe_2(CO)_9$ at 2056 and 2026 cm^{-1}. We attribute this new absorption to $Fe_3(CO)_{12}$, the strongest ν(CO) band of which in hydrocarbon solution reportedly appears at 2046 cm^{-1}: Noack, K. *Helv. Chim. Acta* **1962**, *45*, 1847−1859.

(69) Duve, G.; Fuchs, O.; Overbeck, H. *Organische Chemikalien Hoechst, Lösemittel Hoechst, Ein Handbuch für Laboratorium und Betrieb*; Hoechst AG: Frankfurt a. M., 1976.

(70) Goldman, S. *Can. J. Chem.* **1974**, *52*, 1668−1680.

readily attributed to $Fe_2(CO)_9$. They grow further with concomitant decrease of the absorption at 1950 cm^{-1} within about 1100 μs (Figure 10C). In the last spectrum (Figure 10D), this band has completely vanished and $Fe_2(CO)_9$ is now the only product. Its formation in two stages is clearly recognizable in Figure 10C, the right-hand part of which shows the absorbance changes on an expanded time scale. The rapid growth of the first batch of $Fe_2(CO)_9$ goes along with the complete decay of the $Fe(CO)_4$(solv) absorption at 1986 cm^{-1} and with the concomitant disappearance of a part of the absorption at 1950 cm^{-1}. The much slower growth of the second batch of $Fe_2(CO)_9$ mirrors the further decay at 1950 cm^{-1}. Hence it follows that this latter absorption is associated with a reservoir form of the $Fe(CO)_4$ fragment, $Fe(CO)_4(H_2O)$ being the obvious candidate. It apparently exists with $Fe(CO)_4$(solv) in an equilibrium, from which it is slowly released, Scheme 6. The competitive reactions with $Fe(CO)_5$ and CO yield $Fe_2(CO)_9$ on one hand and lead to the re-formation of some $Fe(CO)_5$ on the other.

The species $Fe(CO)_4(H_2O)$, like other $Fe(CO)_4L$ complexes with *n*-donor ligands,[71,72] should possess a trigonal-bipyramidal structure with the ligand L in an axial position (C_{3v} symmetry; three IR active ν(CO) modes: 2 A_1, E). Taking $Fe(CO)_4(PEt_3)$ as a typical example [three bands at 2048.6 (A_1), 1974.5 (A_1), and 1935.7 (E) cm^{-1} with 1:1.3:8.8 intensity ratio],[73] we assign the strong band at 1950 cm^{-1} and the shoulder at 1964 cm^{-1} to the E and the low-frequency A_1 ν(CO) modes of $Fe(CO)_4(H_2O)$, respectively. The high-frequency A_1 mode of this species, expected around 2050−2060 cm^{-1}, is hidden underneath the strong absorption of $Fe_2(CO)_9$ centered at 2056 cm^{-1} (Figure 10B). Finally, we note a barely discernible shoulder at the low-frequency side of the E mode of $Fe(CO)_4(H_2O)$, which we tentatively attribute to a small amount of *trans*-$Fe(CO)_3(H_2O)_2$ [D_{3h} symmetry; one IR active ν(CO) mode: E′], taking into account that the E′ mode of *trans*-$Fe(CO)_3L_2$ complexes commonly appears at a lower frequency than the E mode of the corresponding $Fe(CO)_4L$.[73]

Flash Photolysis of $Fe(CO)_4(\eta^2$-1,3-butadiene) (2). What remains to be addressed is the intramolecular photosubstitution of one CO by the free vinyl unit of the η^2-coordinated butadiene ligand in the tetracarbonyl complex **2**, which ultimately yields $Fe(CO)_3(\eta^4$-*s*-*cis*-1,3-bd) (**1**). Compound **2** is most easily accessible in pure state if the preparation from $Fe_2(CO)_9$ and 1,3-butadiene and its isolation from the reaction mixture is performed under milder conditions than previously reported.[6] The improved preparation, along with the complementary characterization of **2** by ^1H and ^{13}C NMR spectroscopy, is given in the Experimental Section.

The moderate thermal stability of **2** in hydrocarbon solution at ambient temperature is greatly improved in the presence of added 1,3-butadiene. Even after several days, a solution of **2** in cyclohexane containing, for example, 85 mM free 1,3-butadiene shows virtually no changes in the intensities of the ν(CO) IR spectrum, if kept in the dark. Therefore, such a stock solution is used for the intended investigation into the photolytic behavior of **2**.

Scheme 7

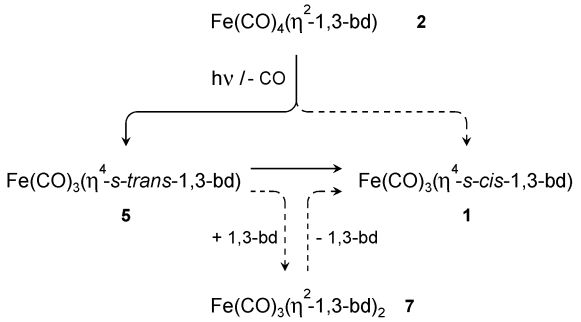

Time-resolved IR spectroscopy with measurements in the micro- and millisecond time ranges reveals that the flash photolysis (λ_{exc} = 308 nm) of **2** initially generates $Fe(CO)_3(\eta^4$-*s*-*trans*-1,3-bd) (**5**) as the major product, which then undergoes η^4-*s*-*trans* → η^4-*s*-*cis* rearrangement to form **1**, Scheme 7.[20]

The ν(CO) pattern of **5** appears almost instantaneously along with the depleted absorptions of the starting material, as observed in an IR difference spectrum recorded 1.2 μs after the flash photolysis of **2**. Virtually no spectral changes occur during the following period of 100 μs, such that a spectrum recorded after 0.1 ms (Figure 11A) is also representative of the initial situation. The assignment of the dominant product absorptions in this spectrum (shaded areas) to $Fe(CO)_3(\eta^4$-*s*-*trans*-1,3-bd) (**5**) is straightforward by comparison with Figures 1C and 2A. The weak absorption at 2054 cm^{-1} is attributed to the high-frequency A′ ν(CO) mode of **1**, which up to this stage is present only in small concentration. The low-frequency A′ and A″ ν(CO) absorptions of **1**, expected at 1988 and 1978 cm^{-1} (cf. Table 1), are canceled due to foot-and-tail overlap with the strong B_2 depletion band of **2** at 1984 cm^{-1}.

A considerable increase in the concentration of **1** occurs subsequently at the expense of **5**, which vanishes completely within a period of about 20 ms, as illustrated in Figure 11B. All three ν(CO) bands of **1** appear well resolved in the resulting difference spectrum (Figure 11C). There is no recovery of the starting material, as manifested by the persisting depletion of **2** at 2082 (A_1) and 2004 cm^{-1} (A_1/B_1).

However, the depletion of the B_2 band of **2** at 1984 cm^{-1} is largely canceled, thus indicating that a new absorption has grown near this position. Bearing in mind that the strongest ν(CO) band of, for example, $Fe(CO)_3(\eta^2$-ethene)$_2$ appears at 1981 cm^{-1},[74] we assume that a product of type $Fe(CO)_3(\eta^2$-1,3-bd)$_2$ (**7**) is formed by addition of 1,3-butadiene to **5** in a side reaction of the **5** → **1** rearrangement, Scheme 7. This side reaction may involve the species $Fe(CO)_3(\eta^2$-1,3-bd) (**3**) as a reactive intermediate, by analogy with the proposal made in Scheme 3 for the formation of a minor amount of $Fe(CO)_4(\eta^2$-1,3-bd) (**2**) as a side product of the **5** → **1** rearrangement under CO atmosphere.

(71) Shriver, D. F.; Whitmire, K. H. In *Comprehensive Organometallic Chemistry*; Wilkinson, G., Stone, G. A., Abel, E. W., Eds.; Pergamon: Oxford, England, 1982; Vol. 4, pp 289−291.
(72) Chen, Y.; Hartmann, M.; Frenking, G. *Z. Anorg. Allg. Chem.* **2001**, *627*, 985−998.
(73) Reckziegel, A.; Bigorgne, M. *J. Organomet. Chem.* **1965**, *3*, 341−354.
(74) Wuu, Y.-M.; Bentsen, J. G.; Brinkley, C. G.; Wrighton, M. S. *Inorg. Chem.* **1987**, *26*, 530−540.

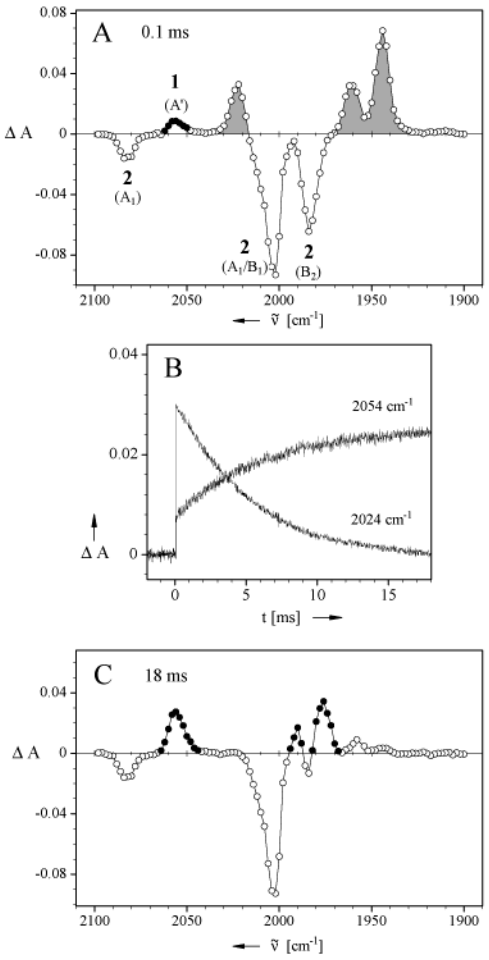

Figure 11. Flash photolysis (λ_{exc} = 308 nm) of $Fe(CO)_4$(η^2-1,3-bd) (**2**, 0.5 mM, in cyclohexane solution containing 85 mM 1,3-butadiene) under argon atmosphere at 25 °C. (A) Transient ν(CO) difference spectrum recorded after 0.1 ms showing the depletion bands of **2** [2082 (A_1), 2004 (A_1/B_1), 1984 cm^{-1} (B_2)] and the absorptions of photogenerated $Fe(CO)_3$(η^4-*s*-*trans*-1,3-bd) (**5**) (2024, 1962, 1944 cm^{-1}; shaded area) along with a weak absorption attributed to $Fe(CO)_3$(η^4-*s*-*cis*-1,3-bd) (**1**) [2054 cm^{-1} (A′); (●)]. (B) Growth of **1** (monitored at 2054 cm^{-1}) with concomitant decay of **5** (monitored at 2024 cm^{-1}). (C) Difference spectrum recorded after 18 ms showing the depletion bands of **2** along with the product pattern of **1** [2054 (A′), 1990 (A′), 1976 cm^{-1} (A″); (●)]; for further details see text.

$Fe(CO)_3$(η^2-olefin)$_2$ complexes are known for their relatively low stability.[74−76] Hence one would expect that a compound of type $Fe(CO)_3$(η^2-1,3-bd)$_2$ (**7**) undergoes intramolecular displacement of one of the two η^2-1,3-butadiene ligands with ultimate formation of an additional amount of **1**, Scheme 7. This is indeed recognizable from a comparison of the transient difference spectrum shown in Figure 11C with an FTIR difference spectrum recorded several minutes later (Figure 12). The intensity of the ν(CO) pattern of **1** in relation to the depleted absorptions of the starting material **2** has increased significantly, while the depletion of the low-frequency B_2 band of **2** is no longer canceled by the absorption associated with species **7**.

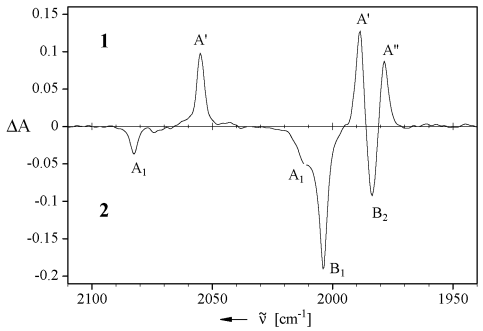

Figure 12. FTIR difference spectrum recorded several minutes after single-flash irradiation (XeCl excimer laser, λ_{exc} = 308 nm; 95 mJ incident flash energy) of $Fe(CO)_4$(η^2-1,3-bd) (**2**, 0.5 mM, in cyclohexane solution containing 85 mM 1,3-butadiene) under argon atmosphere at ambient temperature in an IR cell (d = 1 mm), showing $Fe(CO)_3$-(η^4-1,3-bd) (**1**) as the only product (for frequency data see Table 1).

The changes of ΔA in the 20 ms time window, recorded at 2054 and 2024 cm^{-1} (Figure 11B) and a wide range of other monitoring wavenumbers, show satisfactory fits to first-order kinetics, yielding an average value of k_{obs} = 185 (±10) s^{-1}. These data underline the influence of the concentration of added 1,3-butadiene (85 mM) on the decay of **5**. It is smaller compared with the value found in the presence of 130 mM 1,3-butadiene (250 s^{-1}), where **5** was generated from $Fe(CO)_5$, but much larger than the one evaluated for the **5** → **1** rearrangement in CO-saturated solution in the absence of added 1,3-butadiene (77 s^{-1}, at 25 °C). The acceleration by 1,3-butadiene may in part be due to the additional reaction channel leading to the type **7** product, but this is probably not sufficient to rationalize this effect entirely. One might invoke, for example, a decrease of the activation barrier of the **5** → **1** rearrangement arising from a stabilization of the transition state(s), **TS[5−1]** and/or **TS[5−3]** (Figure 6), by interaction with the diene.[55]

Concluding Remarks

Surveying the observations made in this work, we can distinguish two highlights: the discovery of $Fe(CO)_3$-(η^4-*s*-*trans*-1,3-bd) (**5**) as a transient isomer of the classical $Fe(CO)_3$(η^4-*s*-*cis*-1,3-bd) (**1**) and the detection of the doubly unsaturated fragment $Fe(CO)_3$(solv) as a single-photon product of $Fe(CO)_5$ in addition to $Fe(CO)_4$-(solv). Armed with this information, we are now in a position to present Scheme 8[18,20] as a substantially expanded and revised version of the earlier proposals made for the photochemical synthesis of **1** from $Fe(CO)_5$ and 1,3-butadiene (Scheme 1)[5] and the photolytic behavior of **1** as well.[15,16,77]

The involvement of the η^4-*s*-*trans*-1,3-bd complex **5** as a kinetically favored intermediate in either of the two

(75) Fleckner, H.; Grevels, F.-W.; Hess, D. *J. Am. Chem. Soc.* **1984**, *106*, 2027−2032.
(76) Weiller, B. H.; Miller, M. E.; Grant, E. R. *J. Am. Chem. Soc.* **1987**, *109*, 352−356.

(77) Trapping of the CO loss fragment **4** by potential ligands other than CO is included in the scheme, though such reactions are not dealt with in the present paper. They will be communicated in a forthcoming publication along with the results of current investigations into the photolytic behavior of other $Fe(CO)_3$(η^4-1,3-diene) complexes. Preliminary observations indicate that compounds containing acyclic 1,3-dienes (isoprene, 2,3-dimethyl-1,3-butadiene) expectedly undergo both photolytic CO detachment and η^4-*s*-*cis* → η^4-*s*-*trans* photoisomerization. Here again, the latter process is largely reversible and, hence, has little net effect apart from diminishing the efficiency of CO photosubstitution in accord with previous quantum yield measurements.[15]

Scheme 8

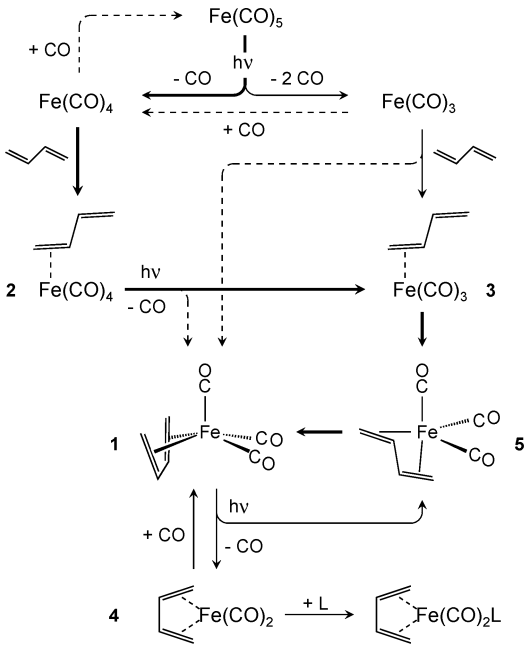

routes from $Fe(CO)_5$ to **1** is readily rationalized as follows. The *s-trans* form is by far the predominant conformer of 1,3-butadiene,[78,79] such that the $Fe(CO)_3$(solv) fragment, if generated in the presence of the diene, preferentially adds this *s-trans* conformer to yield $Fe(CO)_3(\eta^2$-1,3-bd) (**3**) (with $\phi_d = -150.1°$; Figure 3) as the primary adduct.[80] The same species **3** will also be formed by photolytic CO detachment from $Fe(CO)_4(\eta^2$-1,3-bd) (**2**), which contains the diene in a nearly *s-trans* conformation.[81] Separated from **5** by a barrier as low as 0.9 kcal·mol^{-1} (Figure 5), species **3** will immediately move downhill in energy with formation of **5**, which subsequently undergoes η^4-*s-trans* → η^4-*s-cis* rearrangement to yield **1** as the thermodynamically more stable product.

Trapping of the fragments $Fe(CO)_4$(solv) and $Fe(CO)_3$(solv) by unphotolyzed $Fe(CO)_5$ or by trace impurities such as water (Scheme 6) is omitted in Scheme 8, since these processes are negligible for kinetic reasons as long as 1,3-butadiene is present in sufficiently large excess. However, one has to consider undesired $Fe_2(CO)_9$ formation when exploiting the photosubstitution of $Fe(CO)_5$ for preparative purposes in runs with high complex concentrations. It is for this reason that in the preparation of **1** (see Experimental Section) the parent $Fe(CO)_5$ is added in several successive portions to the solution of 1,3-butadiene, by analogy with the procedure proven successful in the synthesis of, for example, $Fe(CO)_3(\eta^2$-(*Z*)-cyclooctene$)_2$.[75] This precaution is particularly necessary in cases where a large excess of the entering ligand is prohibitive for economic reasons.

It is unfortunate that the response time of our instrumentation prevents us from gathering information on the early events in the photofragmentation of $Fe(CO)_5$, prior to the appearance of (singlet) $Fe(CO)_4$(solv) and $Fe(CO)_3$(solv) (Figure 9A). Picosecond studies conducted elsewhere[82] have nevertheless shown that the naked (triplet) $Fe(CO)_4$ is almost instantaneously photogenerated from $Fe(CO)_5$ in heptane solution (where it persists for not less than 600 ps), but no evidence was found for the doubly unsaturated fragment $Fe(CO)_3$. All the more exciting are most recent findings according to which both triplet $Fe(CO)_4$ and $Fe(CO)_3$ are clearly observable in heptane at a time as early as 10 ps.[83]

The occurrence of 2-fold CO photodetachment from $Fe(CO)_5$ is also relevant to reactions other than those specifically dealt with in the present work. Obvious examples are photoinduced carbonyliron-catalyzed processes, such as olefin isomerization or hydrogenation,[85] where the $Fe(CO)_3$ moiety plays a key role as the repeating unit in the catalytic cycle. Another interesting case is the single-photon conversion of $Fe(CO)_5$ into mixtures of mono- and disubstituted derivatives of type $Fe(CO)_4L$ and $Fe(CO)_3L_2$ (L = mono-olefin or phosphorus ligands),[58,84−87] where the addition of two ligands L to the doubly unsaturated $Fe(CO)_3$(solv) fragment can now be considered as the most simple route to the $Fe(CO)_3L_2$ products. Competitive trapping of $Fe(CO)_3$(solv) by $Fe(CO)_5$ may occur in case of high $Fe(CO)_5$:L ratios. This would yield the dinuclear species $Fe_2(CO)_8$ (cf. Scheme 6), which upon reaction with two ligands L can form two $Fe(CO)_4L$ product molecules as the ultimate result of the absorption of one single photon, thus providing a new, simple rationale of quantum yields exceeding unity.[87]

Experimental Section

General Remarks. All reactions and manipulations of the air-sensitive carbonyliron complexes are carried out under argon and in argon-saturated solvents, unless otherwise noted, using standard Schlenck techniques. Spectra are recorded on the following instruments: IR, Perkin-Elmer 1600 FTIR (operating with 2 cm^{-1} resolution), Bruker IFS 66 (operating with 0.5 cm^{-1} resolution); UV−vis, Shimadzu UV-2102PC; NMR, Bruker ARX 250, Bruker DRX 400.

Materials. Synthetic grade *n*-pentane (95%, Merck), 1,3-butadiene (99%, Messer Griesheim), and chloroform-d_1 (99.8%, Deutero GmbH) are used as received. High-purity gases used for the flash photolysis experiments (Ar, ≥99.9999%; CO, ≥99.997) are purchased from Messer Griesheim. Cyclohexane (>99.6%, Fisher Scientific) is refluxed over $LiAlH_4$ for 24 h followed by distillation under argon atmosphere through a 5 m glass-packed column until no impurities are detectable by GC. $Fe(CO)_5$ (>97%, Fluka) is purified by trap-to-trap vacuum distillation prior to use (IR ν(CO) data: see Table 1).

(78) Huber-Wälchli, P. *Ber. Bunsen-Ges. Phys. Chem.* **1978**, *82*, 10−12.
(79) Mui, P. W.; Grunwald, E. *J. Am. Chem. Soc.* **1982**, *104*, 6562−6566.
(80) It is worth mentioning in this context that the involvement of the *s-trans* conformer of a free 1,3-diene was not considered in related gas phase studies.[49] Rather, photogenerated $Fe(CO)_3$ was suggested to add the 1,3-diene in the form of its *s-cis* conformer, yielding an (*s-cis*-1,3-diene)-$Fe(CO)_3$ type complex as the only initially formed adduct.
(81) A geometry optimization of $Fe(CO)_4(\eta^2$-1,3-bd) (**2**) at the BP86 level of DFT was started with a guess derived from the structure of $[Fe(CO)_4]_2(\eta^2{:}\eta^2$-1,3-bd) (Klanderman, K. A. Ph.D. Dissertation, University of Wisconsin, 1965; Dissertation Abstr. **1965**, *25*, 6253) by removal of one $Fe(CO)_4$ unit. The computed structure exhibits a diene dihedral angle of $\phi_d = -161.2°$.
(82) Snee, P. T.; Payne, C. K.; Kotz, K. T.; Yang, H.; Harris, C. B. *J. Am. Chem. Soc.* **2001**, *123*, 2255−2264.
(83) George, M. W. Personal communication.
(84) Angermund, H.; Bandyopadhyay, A. K.; Grevels, F.-W.; Mark. F. *J. Am. Chem. Soc.* **1989**, *111*, 4656−4661.
(85) Schroeder, M. A.; Wrighton, M. S. *J. Am. Chem. Soc.* **1976**, *98*, 551−558.
(86) Nayak, S. K.; Burkey, T. J. *Inorg. Chem.* **1992**, *31*, 1125−1127.
(87) Nayak, S. K.; Farrell, G. J.; Burkey, T. J. *Inorg. Chem.* **1994**, *33*, 2236−2242.

$Fe_2(CO)_9$,[65d] $Fe(CO)_3(\eta^4$-1,3-bd) (**1**),[5] and $Fe(CO)_4(\eta^2$-1,3-bd) (**2**)[6] are prepared according to the published procedures, but with some modifications as described in the following.

$Fe(CO)_3(\eta^4$-1,3-butadiene) (1). A solution of $Fe(CO)_5$ in 1,3-butadiene-saturated *n*-pentane (400 mL), which replaces the toxic benzene solvent used in the published procedure,[5] is irradiated at ambient temperature in a water-cooled immersion-well apparatus[88] (Solidex glass, $\lambda > 280$ nm) equipped with a Philips HPK 125 W high-pressure mercury lamp. The total amount of $Fe(CO)_5$ (15 mL, 21.8 g, 0.11 mol) is added in three portions, according to the progress of the conversion (as monitored by IR), to suppress the formation of $Fe_2(CO)_9$. The irradiation is continued until the starting material is largely consumed (14 h). Vacuum evaporation of the volatiles ($\leq 10^{-2}$ hPa) at ambient temperature, followed by trap-to-trap vacuum distillation of the residue at 40 °C, yields a yellow oil (14.8 g), which upon redistillation using a concentric tube column affords spectroscopically pure **1** (8.1 g, 38%), yellow oil, bp 51 °C at 9 hPa. IR ν(CO): see Table 1. ^{13}C NMR ($CDCl_3$, 300 K): δ 211.82 (CO), 85.59 (d, $^1J_{CH}$ 170 Hz; =*C*H−), 40.82 (t, $^1J_{CH}$ 161 Hz; *C*H_2=).

$Fe(CO)_4(\eta^2$-1,3-butadiene) (2). A suspension of $Fe_2(CO)_9$ (1.21 g, 3.32 mmol) in a solution of 1,3-butadiene (ca. 6 g, ca. 0.11 mol) in *n*-pentane (150 mL) is stirred at ambient temperature in the dark until the insoluble starting complex has vanished (3 h). Evaporation of the volatiles at ≤−30 °C under reduced pressure ($\leq 10^{-2}$ hPa) is continued (ca. 10 h) until $Fe(CO)_5$ is completely removed from the residue (monitored by IR). Vacuum sublimation yields spectroscopically pure **2** as a yellow oil (0.67 g, 90%). IR ν(CO): see Table 1. ^{13}C NMR ($CDCl_3$, 300 K): δ 211.34 (CO), 142.23 (d, $^1J_{CH}$ 153 Hz; CH_2=*C*H−), 112.47 (t, $^1J_{CH}$ 156 Hz; *C*H_2=CH−), 60.46 (d, $^1J_{CH}$ 155 Hz; η^2-CH_2=*C*H−), 36.13 (t, $^1J_{CH}$ 159 Hz; η^2-*C*H_2=CH−). ^{1}H NMR ($CDCl_3$, 263 K): δ 5.70 (m, 1 H), 5.27 (m, 1 H), 4.88 (m, 1 H), 4.02 (m, 1 H), 2.65 (m, 1 H), 2.59 (m, 1 H).

Flash Photolysis with Time-Resolved IR Spectroscopy. The basic design of our instrumentation[89] and details of the actual configuration and performance[90] (HgCdTe photodiode, system response time 1−1.2 μs, 7−8 cm^{-1} spectral resolution) have been described previously. In the present study, the flash energy of the Lambda Physik EMG 200 excimer laser, operating with XeCl for $\lambda = 308$ nm emission (pulse duration 20 ns), is routinely attenuated to 25−30 mJ/pulse. With the chosen concentrations of $Fe(CO)_3(\eta^4$-1,3-bd) (**1**) (1.5 mM), $Fe(CO)_4(\eta^2$-1,3-bd) (**2**) (0.5 mM), and $Fe(CO)_5$ (2 mM) in the 1 mm sample cell, the absorbance at 308 nm ranges from 0.25 to 0.35. Data acquisition for point-by-point construction of transient spectra (every 2 cm^{-1}) and kinetic analysis (using homemade PC software for fitting to a monoexponential function) routinely involves signal averaging of three single-shot experiments. After each laser shot, the thermostated IR cell is emptied and refilled with a fresh portion of the respective stock solution from the reservoir, which is kept under the desired gas atmosphere at 1060 hPa.

Computational Methods. All DFT calculations are carried out by means of the Gaussian 98 package of programs,[91] using Becke's gradient-corrected exchange-energy functional[92] in combination with Perdew's density-functional approximation for the correlation energy,[93] referenced as BP86. For the central iron atom a pseudopotential developed by Stoll and co-workers is used,[94] which simulates the 10 neon shell core electrons of the iron atom, while the remaining 16 valence electrons are described by means of a (8s7p6d1f/6s5p3d1f) basis set. Carbon, oxygen, and hydrogen atoms are treated by means of the 6-31G* basis set.[95] Geometry optimizations are performed in redundant internal coordinates[96] using the GDIIS algorithm (geometry optimization by direct inversion in the iterative subspace).[97] Transition states are searched for by means of the STQN method[98] and finally refined using the regular transition state optimization. Energies are reported with and without zero point energy (ZPE) correction. Frequencies are calculated from analytical second derivatives.

Acknowledgment. This paper is dedicated to Professor Karl Wieghardt on the occasion of his 60th birthday. Skillful technical assistance by P. Bayer, D. Merkl, R. Schrader, and the NMR spectroscopic staff of the MPI für Strahlenchemie is gratefully acknowledged. The authors wish to thank L. J. Currell, Dr. H. Görner, G. Klihm, Dr. W. E. Klotzbücher, and Dr. B. Weimann for their help and advice concerning flash photolysis in combination with time-resolved IR spectroscopy and computer-assisted signal analysis. Particular thanks are due to Dr. M. W. George (University of Nottingham, UK) for disclosing his recent findings prior to publication.

OM020785C

(88) Grevels, F.-W.; Reuvers, J. G. A.; Takats, J. *Inorg. Synth.* **1986**, *24*, 176−180.
(89) Schaffner, K.; Grevels, F.-W. *J. Mol. Struct.* **1988**, *173*, 51−65.
(90) Grevels, F.-W.; Kerpen, K.; Klotzbücher, W. E.; Schaffner, K.; Goddard, R.; Weimann, B.; Kayran, C.; Özkar, S. *Organometallics* **2001**, *20*, 4775−4792.
(91) Frisch, M. J.; Trucks, G. W.; Schlegel, H. B.; Scuseria, G. E.; Robb, M. A.; Cheeseman, J. R.; Zakrzewski, V. G.; Montgomery, J. A., Jr.; Stratmann, R. E.; Burant, J. C.; Dapprich, S.; Millam, J. M.; Daniels, A. D.; Kudin, K. N.; Strain, M. C.; Farkas, O.; Tomasi, J.; Barone, V.; Cossi, M.; Cammi, R.; Mennucci, B.; Pomelli, C.; Adamo, C.; Clifford, S.; Ochterski, J.; Petersson, G. A.; Ayala, P. Y.; Cui, Q.; Morokuma, K.; Malick, D. K.; Rabuck, A. D.; Raghavachari, K.; Foresman, J. B.; Cioslowski, J.; Ortiz, J. V.; Stefanov, B. B.; Liu, G.; Liashenko, A.; Piskorz, P.; Komaromi, I.; Gomperts, R.; Martin, R. L.; Fox, D. J.; Keith, T.; Al-Laham, M. A.; Peng, C. Y.; Nanayakkara, A.; Gonzalez, C.; Challacombe, M.; Gill, P. M. W.; Johnson, B.; Chen, W.; Wong, M. W.; Andres, J. L.; Gonzalez, C.; Head-Gordon, M.; Replogle, E. S.; Pople, J. A. *Gaussian 98*, Revision A.5; Gaussian Inc.: Pittsburgh, PA, 1998.
(92) Becke, A. D. *Phys. Rev. A* **1988**, *38*, 3098−3100.
(93) Perdew, J. P. *Phys. Rev. B* **1986**, *33*, 8822−8824.
(94) See, for example: (a) Dolg, M.; Stoll, H.; Preuss, H. *Theor. Chim. Acta* **1993**, *85*, 441−450, and references therein. (b) Wedig, U.; Dolg, M.; Stoll, H. In *Quantum Chemistry: The Challenge of Transition Metals and Coordination Chemistry*; Veillard, A., Ed.; Reidel: Dordrecht, 1986; pp 79−89. (c) Leininger, T.; Nicklass, A.; Stoll, H.; Dolg, M.; Schwerdtfeger, P. *J. Chem. Phys.* **1996**, *105*, 1052−1059, and references therein.
(95) Hehre, W. J.; Ditchfield, R.; Pople, J. A. *J. Chem. Phys.* **1972**, *56*, 2257−2261.
(96) Peng, C.; Ayala, P. Y.; Schlegel, H. B.; Frisch, M. J. *J. Comput. Chem.* **1996**, *17*, 49−56.
(97) Császár, P.; Pulay, P. *J. Mol. Struct.* **1984**, *114*, 31−34.
(98) Peng, C.; Schlegel, H. B. *Isr. J. Chem.* **1994**, *33*, 449−454.